Research Square

Preprints are preliminary reports that have not undergone peer review.
They should not be considered conclusive, used to inform clinical practice,
or referenced by the media as validated information.

Sickle cell anemia is associated with region-specific alterations in mandibular trabecular bone microarchitecture: a cross-sectional radiographic study

Diego Thiers Oliveira Carneiro
diego_thiers@hotmail.com

Federal University of Ceará
Howard Lopes Ribeiro Júnior
Federal University of Ceará
Ana Clara Costa
Federal University of Ceará
Fábio Wildson Gurgel Costa
Federal University of Ceará
Luan Rebouças Castelo
Federal University of Ceará
Adriano Evangelista Maia
Federal University of Ceará
Suzzy Maria Carvalho Dantas
Federal University of Ceará
Romélia Pinheiro Gonçalves Lemes
Federal University of Ceará

Research Article

Keywords: Sickle cell anemia, Panoramic radiography, Trabecular bone

Posted Date: November 6th, 2026

DOI: https://doi.org/10.21203/rs.3.rs-11406819/v1

License: This work is licensed under a Creative Commons Attribution 4.0 International License. Read Full License

Additional Declarations: No competing interests reported.

Abstract

Background

Sickle cell anemia (SCA) is a genetic disorder characterized by altered red blood cell morphology, leading to multiple systemic manifestations, including changes in bone microarchitecture associated with chronic hemolysis, compensatory bone marrow expansion, and altered bone remodeling. This study aimed to characterize mandibular trabecular bone through quantitative panoramic radiographic analysis, comparing patients with SCA and systemically healthy controls across age groups, and to investigate associations with hematological and biochemical markers in patients with SCA.

Methods

This cross-sectional observational study included 50 patients with SCA and 50 systemically healthy controls matched by age and sex, stratified into two age groups (18–29 and ≥ 30 years). Three mandibular regions of interest (50 × 50 pixels) were analyzed using ImageJ to assess mean pixel intensity, fractal dimension, lacunarity, and trabecular morphometric and connectivity parameters. Statistical analyses included between-group comparisons, two-way analysis of variance, and Spearman correlations, with Benjamini–Hochberg correction for multiple comparisons.

Results

The median age was 32.5 years, and 68% of participants were female. Patients with SCA aged 18–29 years showed lower mean pixel intensity in the mandibular ramus (ROI1) than controls (mean difference = − 31.16; adjusted $p = 0.006$). Fractal dimension was also lower in ROI1 among participants aged 18–29 years (adjusted $p = 0.033$) and ≥ 30 years (adjusted $p = 0.014$). Lacunarity showed no significant between-group differences after multiple-comparison correction (adjusted $p > 0.05$), although a group-by-age interaction was observed in the molar region (ROI2; $p = 0.011$). Among participants aged ≥ 30 years, normalized morphometric parameters were reduced, including the trabecular perimeter-to-total area ratio in ROI1 (adjusted $p < 0.001$) and ROI3 (adjusted $p = 0.007$), and the trabecular length-to-trabecular area ratio in ROI1 (adjusted $p = 0.019$). No associations between radiographic parameters and laboratory markers remained statistically significant after correction (adjusted $p \geq 0.05$).

Conclusions

SCA was associated with radiographic alterations in mandibular trabecular bone, characterized by lower pixel intensity, reduced fractal complexity, and morphometric changes in trabecular extent and organization. Lacunarity showed age-dependent variation without consistent between-group differences. These findings suggest impaired mandibular trabecular bone organization associated with SCA, with patterns varying across anatomical regions and age groups, without confirmed associations with laboratory markers.

1. Introduction

Sickle cell anemia (SCA) is a hereditary hemoglobin disorder caused by a point mutation in the β-globin gene (HBB), resulting in the production of abnormal hemoglobin S (HbS). Under low oxygen tension, HbS polymerizes, promoting red blood cell sickling, chronic hemolysis, and vaso-occlusion [1, 2]. These mechanisms trigger endothelial dysfunction, oxidative stress, and persistent inflammation, contributing to progressive multiorgan damage and substantial morbidity throughout life [1–3]. In addition to its hematological and vascular manifestations, SCA affects bone metabolism and skeletal integrity through mechanisms associated with chronic anemia, compensatory erythropoietic activity, recurrent hypoxia, and altered bone remodeling [4, 5].

Bone involvement in SCA is multifactorial and may result from an imbalance between bone formation and resorption. Chronic hemolytic anemia increases erythropoietic demand, stimulating bone marrow hyperplasia and expansion of medullary spaces. Concurrently, tissue hypoxia, vaso-occlusive events, inflammatory mediators, and oxidative stress may impair osteoblast function and promote osteoclast activity, contributing to alterations in bone mass and trabecular organization [4–6]. These mechanisms have been associated with reduced bone mineral density, osteonecrosis, and other skeletal complications, suggesting that bone impairment in SCA involves both quantitative and structural changes [4, 5].

The systemic mechanisms underlying skeletal impairment in SCA may also be reflected in hematological and biochemical markers. Hemoglobin concentration reflects the severity of anemia, whereas fetal hemoglobin (HbF) is an important modifier of disease severity because it inhibits HbS polymerization and reduces sickling-related complications [7]. Markers of hemolysis, including lactate dehydrogenase, bilirubin, aspartate aminotransferase, and reticulocyte count, provide complementary information on hemolytic activity [8]. In addition, abnormalities in iron metabolism, systemic inflammation, and bone turnover may contribute to skeletal alterations. Serum ferritin and transferrin saturation provide information related to iron status, while alkaline phosphatase may reflect bone remodeling activity, although total alkaline phosphatase is not specific to bone tissue [5, 9]. Increased osteoclast activity has also been associated with inflammatory mechanisms in SCA [9]. These findings provide a biological rationale for investigating whether systemic laboratory markers are associated with local mandibular trabecular characteristics.

The maxillofacial skeleton may also be affected by these systemic mechanisms. Oral manifestations of SCA include dental abnormalities, pulp alterations, changes in the periodontal supporting structures, and abnormalities of the maxillary and mandibular bones [10]. In the jaws, compensatory bone marrow expansion may increase medullary spaces and modify trabecular thickness, distribution, and organization. Radiographically, these alterations may manifest as enlarged marrow spaces, irregular trabeculation, and changes in the structural pattern of cancellous bone [10, 11]. Previous

investigations have identified increased intertrabecular spacing, changes in fractal characteristics, and a higher prevalence of trabecular abnormalities in the maxilla and mandible of individuals with SCA compared with healthy controls [10–12]. These findings indicate that the disease may influence mandibular bone organization beyond clinically evident skeletal complications.

Quantitative analysis of dental radiographs provides an opportunity to investigate these alterations through complementary structural measurements. Mean pixel intensity reflects the grayscale characteristics of radiographic images, whereas fractal dimension estimates the complexity of the projected trabecular pattern. Lacunarity provides additional information regarding spatial heterogeneity and the distribution of gaps within the analyzed structure [13, 14]. Morphometric measurements, including trabecular area, perimeter, length, terminal points, and junction elements, further characterize the extent and organization of the trabecular network [14]. When applied together, these parameters may provide a more comprehensive characterization of radiographic trabecular features than conventional visual assessment alone.

The combined evaluation of pixel intensity, fractal dimension, lacunarity, and morphometric connectivity parameters across different mandibular regions and age groups, together with their potential relationships with hematological and biochemical markers, remains insufficiently explored [15]. Therefore, this study aimed to characterize mandibular trabecular bone using quantitative panoramic radiographic analysis, comparing patients with SCA and systemically healthy controls across age groups, and to investigate associations between radiographic parameters and hematological and biochemical markers exclusively among patients with SCA.

2. Material and Methods

2.1 Study design and participants

This cross-sectional observational study included 100 adult participants: 50 patients diagnosed with sickle cell anemia (SCA group), followed at the Hematology and Hemotherapy Center of Ceará (HEMOCE), Brazil, and 50 systemically healthy individuals (healthy controls, HC group). Participants were recruited between January 2024 and July 2026. A convenience sample was assembled from eligible adults with SCA who had a digital panoramic radiograph available in their medical records and hematological and biochemical examinations obtained within a maximum interval of 2 months from the radiographic examination. No a priori sample-size calculation was performed. Healthy controls were individually selected in a 1:1 ratio to match participants with SCA according to age and sex. This matching was used during participant selection to obtain comparable group distributions; matched pairs were not retained as analytical units. Individuals reporting alcohol consumption or smoking were excluded based on medical records. Participants were stratified into two age categories (18–29 and ≥ 30 years), considering the transition between peak bone mass acquisition and skeletal maturity [16].

2.2 Radiographic acquisition and image standardization

Digital panoramic radiographs were obtained using a Kodak K9000 3D system (Kodak Dental Systems, Carestream Health, Rochester, NY, USA), with 14-bit grayscale resolution, an exposure time of 13.9 s, 65 kV, and 10 mA. Patient positioning was standardized using chin and head supports, with the Frankfurt horizontal plane parallel to the floor and the midsagittal plane perpendicular to the floor, following established panoramic radiographic procedures [14].

Images were stored in Tagged Image File Format (TIFF) and processed using ImageJ software (version 1.53, National Institutes of Health, Bethesda, MD, USA) [17]. To standardize image dimensions, the height was set to 1536 pixels while preserving the original aspect ratio, avoiding geometric distortion during processing.

2.3 Selection and preparation of regions of interest

Three standardized regions of interest (ROIs), each measuring 50 × 50 pixels, were selected on the right side of the mandible using the rectangular selection tool in ImageJ, based on previously described mandibular texture analysis approaches [13, 14].

ROI1 was positioned at the geometric center of the mandibular ramus. ROI2 was located below and between the roots of the first and second mandibular molars; when these teeth were absent, an alternative position was established 2 cm horizontally from the intersection of the oblique line and mandibular ramus. ROI3 was selected between the mental foramen and the inferior mandibular cortex.

The same ROIs were used for mean pixel intensity, fractal dimension, lacunarity, and complementary morphometric analyses. ROI positioning and the image-processing workflow are illustrated in Figure. 1. To minimize potential measurement bias, all panoramic radiographs were obtained using the same equipment and standardized acquisition protocol, and identical ROI dimensions, anatomical positioning criteria, and image-processing procedures were applied to both study groups.

2.4 Quantitative assessment of mean pixel intensity

Mean pixel intensity (MPI) was quantified individually in each ROI using the Histogram function in ImageJ [18]. The arithmetic mean of the grayscale values, reported as "Mean" by the software, was recorded as the quantitative radiographic intensity parameter. In 8-bit grayscale images, pixel intensity ranges from 0 (black) to 255 (white), with higher values indicating greater image brightness or radiopacity.

To complement the quantitative assessment, the same ROIs were analyzed using the Surface Plot function, which provides a three-dimensional representation of the spatial distribution of grayscale values [18]. The horizontal axes correspond to the ROI dimensions, whereas the vertical axis

represents pixel intensity. This visualization was used exclusively for qualitative characterization of intensity distribution and did not constitute an independent quantitative outcome.

2.5 Fractal dimension analysis

Fractal dimension (FD) was calculated to estimate the complexity of the projected mandibular trabecular pattern, following the image-processing approach described by White and Rudolph and supported by previous quantitative studies of mandibular bone texture [14, 19].

Each ROI was duplicated and subjected to Gaussian blurring (35-pixel diameter). The blurred image was subtracted from the original image, and a grayscale value of 128 was added. The resulting image was binarized, inverted, eroded, dilated, and skeletonized. Fractal dimension was subsequently calculated using the box-counting method in ImageJ.

This standardized procedure was applied to all ROIs in both the SCA and HC groups.

2.6 Lacunarity analysis

Lacunarity was assessed as a complementary parameter of spatial heterogeneity and gap distribution within the mandibular trabecular pattern. Previously binarized ROIs were analyzed using the FracLac plugin for ImageJ, following the box-counting approach described by Karperien and applied in mandibular bone texture investigations [13, 14, 20].

The analysis was performed using the FracLac box-counting mode, with the grayscale differential option (Gray 1: Differential), white-background configuration, and nine grid positions. The resulting lacunarity value was recorded for each ROI and used for comparisons between groups and age categories.

2.7 Trabecular morphometric and connectivity analysis

Complementary morphometric analysis was performed to characterize trabecular quantity, extent, and connectivity, based on quantitative mandibular bone imaging approaches, particularly those described by de Sá Cavalcante et al. [14].

Before measurement, radiographic images were spatially calibrated in ImageJ using a reference of known dimensions. The Analyze > Set Scale function was used to establish the relationship between pixel distance and millimeters, maintaining a pixel aspect ratio of 1.0. Linear and area measurements were then expressed in millimeters and square millimeters, respectively.

Trabecular area (A) and perimeter (P) were obtained from binary images, with the perimeter determined after application of the Outline function. Trabecular length (L) was obtained from skeletonized images, while terminal points (E) and junction pixels (J) were identified using the Analyze Skeleton (2D/3D) plugin [14, 21].

In addition to absolute measurements, normalized morphometric ratios were calculated using the total ROI area (T), trabecular area, perimeter, length, terminal points, and junction pixels. These ratios were used to characterize the relative distribution, extent, and connectivity of the trabecular network and to compare structural characteristics between the SCA and HC groups.

2.8 Hematological and biochemical parameters

Hematological and biochemical variables were evaluated exclusively in the SCA group. Laboratory data were retrieved from medical records and included hemoglobin concentration, fetal hemoglobin (HbF), ferritin, transferrin saturation, alkaline phosphatase, total leukocyte count, and neutrophil count. Only laboratory examinations performed within a maximum interval of 2 months of the panoramic radiographic examination were included.

A composite hemolysis index was constructed using lactate dehydrogenase, aspartate aminotransferase, total bilirubin, and reticulocyte count. After transformation and standardization of laboratory measurements, principal component analysis was performed, and the first principal component was used as the hemolysis index. Higher index values represented greater estimated hemolytic activity, following previously described approaches [8].

Associations between laboratory markers and radiographic parameters were investigated exclusively within the SCA group.

2.9 Statistical analysis

Categorical variables were summarized as frequencies and percentages, and continuous variables as means ± standard deviations (SDs) or medians and interquartile ranges (IQRs), as appropriate. There were no missing data for any variables included in the analyses; therefore, no imputation procedures were required.

. Analyses were conducted separately for ROI1, ROI2, and ROI3 and for the age categories of 18–29 and ≥ 30 years. Although HC participants were individually selected to match participants with SCA by age and sex, matching was used only during participant selection. Therefore, all inferential analyses were performed using independent samples.

Normality was assessed using the Shapiro–Wilk test. Mean pixel intensity, fractal dimension, lacunarity, trabecular area, perimeter, length, and normalized trabecular parameters were compared using Welch's t-test. Endpoints and junction pixels were compared using the Mann–Whitney U test. Hedges' g with 95% confidence intervals was calculated for mean pixel intensity, fractal dimension, and lacunarity. Two-way ANOVA was used to evaluate the main effects of study group and age category and their interaction for mean pixel intensity, fractal dimension, and lacunarity.

Within the SCA group, associations between laboratory markers and radiographic parameters were assessed using Spearman's rank correlation coefficient, overall and stratified by age category. The hemolysis index was derived by principal component analysis of log-transformed and standardized lactate dehydrogenase, aspartate aminotransferase, total bilirubin, and reticulocyte count. Differences in the hemolysis index between age categories were assessed using the Mann–Whitney U test.

Multiple comparisons were adjusted using the Benjamini–Hochberg false discovery rate (FDR) procedure. FDR correction was applied separately to the 12 pairwise comparisons for each texture outcome, 30 comparisons for absolute morphometric parameters, 84 comparisons for normalized parameters, and 15 correlations for each laboratory marker and analysis stratum. Two-way ANOVA p-values were not included in the FDR adjustment. All tests were two-sided; p-FDR < 0.05 was considered statistically significant for pairwise comparisons and correlations, whereas $p < 0.05$ was used for the two-way ANOVA.

3. Results

3.1 Characteristics of the study population

The study population comprised 100 participants, including 50 individuals with sickle cell anemia (SCA) and 50 systemically healthy controls (HC). The median age was 32.5 years (interquartile range [IQR], 26.0–42.0) in both groups. In each group, 17 participants (34.0%) were aged 18–29 years, whereas 33 (66.0%) were aged ≥ 30 years. Women accounted for 34 participants (68.0%) in each group, while men accounted for 16 (32.0%). These identical age and sex distributions reflect the matching procedure used during participant selection. The epidemiological characteristics of the study population are summarized in Table 1. No data were missing for the demographic, radiographic, hematological, or biochemical variables included in their respective analyses.

Table 1
Epidemiological characteristics and descriptive statistics of mean pixel intensity in the study population.

Characteristic	HC (n = 50)	SCA (n = 50)
Age, years, median (IQR)	32.5 (26.0–42.0)	32.5 (26.0–42.0)
Age group, n (%)		
18–29 years	17 (34.0)	17 (34.0)
≥ 30 years	33 (66.0)	33 (66.0)
Sex, n (%)		
Female	34 (68.0)	34 (68.0)
Male	16 (32.0)	16 (32.0)
Mean pixel intensity, mean ± SD		
18–29 years (n = 17 per group)		
ROI1	151.11 ± 17.78	119.95 ± 27.43
ROI2	74.01 ± 17.05	69.74 ± 18.24
ROI3	74.93 ± 21.65	74.64 ± 25.79
≥ 30 years (n = 33 per group)		
ROI1	142.28 ± 24.18	134.24 ± 27.77
ROI2	90.48 ± 22.47	78.36 ± 21.39
ROI3	85.53 ± 23.62	82.41 ± 27.19

Legend

IQR, interquartile range; ROI, region of interest; SD, standard deviation; SCA, sickle cell anemia.

Mean pixel intensity was evaluated across three regions of interest (ROIs), stratified by study group and age category. In ROI1, mean pixel intensity was higher in controls than in participants with SCA in both age categories. Among participants aged 18–29 years, the respective means were 151.11 ± 17.78 and 119.95 ± 27.43, whereas among those aged ≥ 30 years, they were 142.28 ± 24.18 and 134.24 ± 27.77. In ROI2, mean pixel intensity was also higher in controls in both age categories, with values of 74.01 ± 17.05 versus 69.74 ± 18.24 among participants aged 18–29 years and 90.48 ± 22.47 versus 78.36 ± 21.39 among those aged ≥ 30 years. In ROI3, mean pixel intensity was similar between groups among younger participants (74.93 ± 21.65 in controls versus 74.64 ± 25.79 in the SCA group). Among participants aged ≥ 30 years, the corresponding means were 85.53 ± 23.62 and 82.41 ± 27.19. The descriptive statistics for all three ROIs, stratified by age category and study group, are presented in Table 1. Figure 2 presents surface plots illustrating the

spatial distribution of mean pixel intensity across the three ROIs, stratified by study group and age category. These plots complement the quantitative results in Table 1, with color gradients representing pixel intensity variations within each ROI.

3.2 ROI Pixel Intensity by Study Group and Age

Pairwise comparisons of pixel intensity across the three regions of interest (ROIs) revealed differences according to study group and age category (Table 2). In ROI1, pixel intensity was significantly lower in participants with sickle cell anemia (SCA) than in controls aged 18–29 years (mean difference = − 31.16; false discovery rate [FDR]-adjusted p = 0.006; Hedges' g = − 1.31) (Table 2). No significant differences between age categories were observed within either group, and the comparison between SCA and control participants aged ≥ 30 years was not significant after FDR adjustment (Table 2). In ROI2, controls aged ≥ 30 years had significantly higher pixel intensity than controls aged 18–29 years (mean difference = − 16.47 for the younger-minus-older comparison; FDR-adjusted p = 0.036; Hedges' g = − 0.81) (Table 2). No significant age-related difference was observed within the SCA group. Although pixel intensity was lower in participants with SCA than in controls aged ≥ 30 years, this difference was not statistically significant after FDR adjustment (p = 0.113) (Table 2). No statistically significant pairwise differences were identified in ROI3 (Table 2).

Table 2
Pairwise comparisons and two-way ANOVA of ROI pixel intensity by study group and age category.

ROI	Comparison or effect	Mean difference / *F*statistic	*p*value	FDR-adjusted *p*value	Hedges' *g* (95% CI)
ROI1	SCA, younger vs. older participants [a]	−14.28	0.092	0.257	−0.51 (− 1.09 to 0.08)
	Control, younger vs. older participants [a]	8.84	0.150	0.257	0.41 (− 0.15 to 0.96)
	SCA vs. control, ages 18–29 years [a]	−31.16	< 0.001	**0.006**	−1.31 (− 2.04 to − 0.56)
	SCA vs. control, ages ≥ 30 years [a]	−8.04	0.214	0.321	−0.31 (− 0.78 to 0.18)
	Main effect of study group [b]	10.03	0.002	-	-
	Main effect of age category [b]	0.26	0.609	-	-
	Study group × age category [b]	4.76	0.032	-	-
ROI2	SCA, younger vs. older participants [a]	−8.62	0.144	0.257	−0.42 (− 0.99 to 0.14)
	Control, younger vs. older participants [a]	−16.47	0.006	**0.036**	−0.81 (− 1.38 to − 0.23)
	SCA vs. control, ages 18–29 years [a]	−4.26	0.486	0.584	−0.24 (− 0.89 to 0.42)
	SCA vs. control, ages ≥ 30 years [a]	−12.12	0.028	0.113	−0.55 (− 1.03 to − 0.06)
	Main effect of study group [b]	5.25	0.024	-	-
	Main effect of age category [b]	8.32	0.005	-	-
	Study group × age category [b]	0.81	0.369	-	-
ROI3	SCA, younger vs. older participants [a]	−7.76	0.329	0.439	−0.29 (− 0.86 to 0.29)
	Control, younger vs. older participants [a]	−10.60	0.121	0.257	−0.46 (− 1.03 to 0.12)
	SCA vs. control, ages 18–29 years [a]	−0.29	0.972	0.972	−0.01 (− 0.67 to 0.64)
	SCA vs. control, ages ≥ 30 years [a]	−3.13	0.620	0.676	−0.12 (− 0.60 to 0.36)
	Main effect of study group [b]	0.19	0.666	-	-
	Main effect of age category [b]	3.05	0.084	-	-
	Study group × age category [b]	0.07	0.788	-	-

Legend: ANOVA, analysis of variance; CI, confidence interval; FDR, false discovery rate; ROI, region of interest; SCA, sickle cell anemia. Notes: Pairwise comparisons were performed using Welch's t test. "Younger" refers to participants aged 18–29 years and "older" to those aged ≥ 30 years. For age comparisons, the mean difference was calculated as younger minus older; for comparisons between study groups, it was calculated as SCA minus control. [a] FDR-adjusted p values apply to pairwise comparisons. [b]The two-way ANOVA assessed the main effects of study group and age category and their interaction. For ANOVA, the reported statistic is F; for pairwise comparisons, it is the mean difference. Statistical significance in bold was defined as $p < 0.05$.

Two-way analysis of variance further evaluated the main effects of study group and age category and their interaction (Table 2). In ROI1, a significant main effect of study group was observed ($F = 10.03$, $p = 0.002$), together with a significant group-by-age interaction ($F = 4.76$, $p = 0.032$) (Table 2). The main effect of age category was not significant ($F = 0.26$, $p = 0.609$), suggesting that the difference between study groups varied according to age category. In ROI2, significant main effects were observed for study group ($F = 5.25$, $p = 0.024$) and age category ($F = 8.32$, $p = 0.005$), whereas their interaction was not significant ($F = 0.81$, $p = 0.369$) (Table 2). In ROI3, neither study group ($F = 0.19$, $p = 0.666$) nor age category ($F = 3.05$, $p = 0.084$) had a statistically significant main effect, and the interaction was also not significant ($F = 0.07$, $p = 0.788$) (Table 2).

3.3 ROI Lacunarity by Study Group and Age Category

Lacunarity was evaluated across the three regions of interest (ROIs) according to study group and age category (Table 3). In ROI1, mean lacunarity was slightly higher in the SCA group than in controls among participants aged 18–29 years (0.5449 ± 0.2245 vs. 0.5304 ± 0.2528). Among participants aged ≥ 30 years, the opposite pattern was observed, with lower mean lacunarity in the SCA group than in controls (0.4724 ± 0.1477 vs. 0.5391 ± 0.1134). None of the pairwise comparisons remained statistically significant after false discovery rate (FDR) adjustment. In ROI2, mean lacunarity was higher in the SCA group than in controls among participants aged 18–29 years (0.5771 ± 0.1643 vs. 0.4689 ± 0.1471), whereas among those aged ≥ 30 years, mean lacunarity was lower in the SCA group than in controls (0.5130 ± 0.1674 vs. 0.6014 ± 0.2134). No pairwise comparison remained statistically significant after FDR adjustment. However, two-way analysis of variance (ANOVA) revealed a significant interaction between study group and age category ($F = 6.64$, $p = 0.011$), indicating that the difference in lacunarity between the study groups varied according to age category. Neither the main effect of study group ($p = 0.552$) nor that of age category ($p = 0.372$) was statistically significant (Table 3).

Table 3
Lacunarity in SCA and control groups by age category and region of interest.

Descriptive statistics					
Age category	**ROI**	**Sickle cell disease, mean ± SD**	**Control, mean ± SD**		
18–29 years (n = 17/group)	ROI1	0.5449 ± 0.2245	0.5304 ± 0.2528		
	ROI2	0.5771 ± 0.1643	0.4689 ± 0.1471		
	ROI3	0.5137 ± 0.1586	0.5115 ± 0.1281		
≥ 30 years (n = 33/group)	ROI1	0.4724 ± 0.1477	0.5391 ± 0.1134		
	ROI2	0.5130 ± 0.1674	0.6014 ± 0.2134		
	ROI3	0.4831 ± 0.1477	0.5699 ± 0.1405		
Pairwise comparisons					
ROI	**Comparison**	**Mean difference**	**Raw p-value**	**FDR-adjusted p-value**	**Hedges' g (95% CI)**
ROI1	Sickle cell anemia: 18–29 vs ≥ 30 years	0.0725	0.240	0.361	0.40 (− 0.18 to 0.98)
ROI1	Control: 18–29 vs ≥ 30 years	−0.0087	0.894	0.965	−0.05 (− 0.63 to 0.53)
ROI1	Sickle cell anemia vs control, 18–29 years	0.0145	0.861	0.965	0.06 (− 0.60 to 0.72)
ROI1	Sickle cell anemia vs control, ≥ 30 years	−0.0667	0.044	0.155	−0.50 (− 0.99 to − 0.02)
ROI2	Sickle cell anemia: 18–29 vs ≥ 30 years	0.0641	0.203	0.348	0.38 (− 0.20 to 0.96)
ROI2	Control: 18–29 vs ≥ 30 years	−0.1325	0.014	0.104	−0.67 (− 1.26 to − 0.08)
ROI2	Sickle cell anemia vs control, 18–29 years	0.1082	0.052	0.155	0.68 (0.00 to 1.35)
ROI2	Sickle cell anemia vs control, ≥ 30 years	−0.0884	0.066	0.158	−0.46 (− 0.94 to 0.03)
ROI3	Sickle cell anemia: 18–29 vs ≥ 30 years	0.0306	0.513	0.684	0.20 (− 0.38 to 0.78)
ROI3	Control: 18–29 vs ≥ 30 years	−0.0583	0.149	0.298	−0.42 (− 1.00 to 0.16)
ROI3	Sickle cell anemia vs control, 18–29 years	0.0022	0.965	0.965	0.01 (− 0.64 to 0.67)
ROI3	Sickle cell anemia vs control, ≥ 30 years	−0.0868	0.017	0.104	−0.59 (− 1.08 to − 0.11)
Two-way ANOVA					
ROI	**Effect**	**df**	**F-value**	**p-value**	
ROI1	Study group	1	1.25	0.266	
ROI1	Age category	1	0.75	0.389	
ROI1	Study group × age category	1	1.21	0.274	
ROI2	Study group	1	0.36	0.552	
ROI2	Age category	1	0.80	0.372	
ROI2	Study group × age category	1	6.64	**0.011**	
ROI3	Study group	1	3.84	0.053	

Legend. SD, standard deviation; CI, confidence interval; FDR, false discovery rate; ROI, region of interest. Pairwise comparisons were performed using Welch's t-test. For within-group comparisons, mean differences were calculated as the 18–29-year group minus the ≥ 30-year group; for between-group comparisons, differences were calculated as the sickle cell disease group minus the control group. P-values were adjusted for multiple comparisons using the Benjamini–Hochberg procedure. Hedges' g was used to estimate standardized effect sizes. Two-way ANOVA assessed the main effects of study group and age category and their interaction. All tests were two-sided; $p < 0.05$ was considered statistically significant.

Descriptive statistics				
Age category	**ROI**	**Sickle cell disease, mean ± SD**	**Control, mean ± SD**	
ROI3	Age category	1	0.21	0.650
ROI3	Study group × age category	1	2.14	0.147

Legend. SD, standard deviation; CI, confidence interval; FDR, false discovery rate; ROI, region of interest. Pairwise comparisons were performed using Welch's t-test. For within-group comparisons, mean differences were calculated as the 18–29-year group minus the ≥ 30-year group; for between-group comparisons, differences were calculated as the sickle cell disease group minus the control group. P-values were adjusted for multiple comparisons using the Benjamini–Hochberg procedure. Hedges' g was used to estimate standardized effect sizes. Two-way ANOVA assessed the main effects of study group and age category and their interaction. All tests were two-sided; $p < 0.05$ was considered statistically significant.

In ROI3, mean lacunarity was similar between groups among participants aged 18–29 years (0.5137 ± 0.1586 in the SCA group vs. 0.5115 ± 0.1281 in controls). Among participants aged ≥ 30 years, mean lacunarity was lower in the SCA group than in controls (0.4831 ± 0.1477 vs. 0.5699 ± 0.1405). The unadjusted pairwise comparison for this age category was statistically significant ($p = 0.017$; Hedges' g = − 0.59, 95% CI: −1.08 to − 0.11), but the difference did not remain statistically significant after FDR adjustment ($p = 0.104$). No statistically significant main effects or group-by-age interaction were observed in the two-way ANOVA for ROI3. The principal finding was the significant group-by-age interaction in ROI2 (Table 3).

3.4 Fractal Dimension by Region of Interest, Study Group, and Age Category

Fractal dimension was evaluated across the three regions of interest (ROIs) according to study group and age category (Table 4). In ROI1, mean fractal dimension was lower in the SCA group than in controls among participants aged 18–29 years (1.1999 ± 0.1005 vs. 1.3015 ± 0.0981) and those aged ≥ 30 years (1.2326 ± 0.1024 vs. 1.3170 ± 0.0998). Pairwise comparisons confirmed that these differences remained statistically significant after false discovery rate (FDR) adjustment (18–29 years: mean difference = − 0.1016, adjusted $p = 0.033$; ≥30 years: mean difference = − 0.0844, adjusted $p = 0.014$). Consistently, two-way analysis of variance (ANOVA) identified a significant main effect of study group ($F = 19.21$, $p < 0.001$), with no significant main effect of age category ($p = 0.259$) or group-by-age interaction ($p = 0.686$) (Table 4).

Table 4
Fractal dimension in SCA and control groups by age category and region of interest.

Descriptive statistics					
Age category	**ROI**	**Sickle cell anemia, mean ± SD**	**Control, mean ± SD**		
18–29 years (n = 17/group)	ROI1	1.1999 ± 0.1005	1.3015 ± 0.0981		
	ROI2	1.2282 ± 0.0748	1.2975 ± 0.0885		
	ROI3	1.2531 ± 0.0884	1.2602 ± 0.1088		
≥ 30 years (n = 33/group)	ROI1	1.2326 ± 0.1024	1.3170 ± 0.0998		
	ROI2	1.2688 ± 0.0923	1.3261 ± 0.0911		
	ROI3	1.2579 ± 0.0669	1.2966 ± 0.0800		
Pairwise comparisons					
ROI	**Comparison**	**Mean difference**	**Raw p-value**	**FDR-adjusted p-value**	**Hedges' g (95% CI)**
ROI1	SCA: 18–29 vs. ≥30 years	−0.0327	0.287	0.388	−0.32 (− 0.90 to 0.27)
ROI1	Control: 18–29 vs. ≥30 years	−0.0155	0.603	0.723	−0.15 (− 0.74 to 0.43)
ROI1	SCA vs. control, 18–29 years	−0.1016	**0.005**	**0.033**	−1.00 (− 1.71 to − 0.28)
ROI1	SCA vs. control, ≥ 30 years	−0.0844	**0.001**	**0.014**	−0.82 (− 1.33 to − 0.32)
ROI2	SCA: 18–29 vs. ≥30 years	−0.0406	0.102	0.203	−0.46 (− 1.05 to 0.13)
ROI2	Control: 18–29 vs. ≥30 years	−0.0286	0.291	0.388	−0.31 (− 0.90 to 0.28)
ROI2	SCA vs. control, 18–29 years	−0.0693	0.019	0.058	−0.83 (− 1.53 to − 0.12)
ROI2	SCA vs. control, ≥ 30 years	−0.0573	0.014	0.054	−0.62 (− 1.11 to − 0.12)
ROI3	SCA: 18–29 vs. ≥30 years	−0.0048	0.845	0.845	−0.06 (− 0.65 to 0.52)
ROI3	Control: 18–29 vs. ≥30 years	−0.0364	0.234	0.388	−0.40 (− 0.99 to 0.19)
ROI3	SCA vs. control, 18–29 years	−0.0071	0.836	0.845	−0.07 (− 0.74 to 0.60)
ROI3	SCA vs. control, ≥ 30 years	−0.0387	0.037	0.089	−0.52 (− 1.01 to − 0.03)
Two-way ANOVA					
ROI	**Effect**	**df**	**F-value**	**p-value**	
ROI1	Study group	1	19.21	**< 0.001**	
ROI1	Age category	1	1.29	0.259	
ROI1	Study group × age category	1	0.16	0.686	
ROI2	Study group	1	11.46	**0.001**	
ROI2	Age category	1	3.43	0.067	
ROI2	Study group × age category	1	0.10	0.749	

Legend. SD, standard deviation; CI, confidence interval; FDR, false discovery rate; ROI, region of interest; SCA, sickle cell anemia. Pairwise comparisons were performed using Welch's t-test. For within-group comparisons, mean differences were calculated as the 18–29-year group minus the ≥ 30-year group; for between-group comparisons, differences were calculated as the SCA group minus the control group. P-values were adjusted for multiple comparisons using the Benjamini–Hochberg procedure. Hedges' g was used to estimate standardized effect sizes. Two-way ANOVA assessed the main effects of study group and age category and their interaction. All tests were two-sided; $p < 0.05$ in bold was considered statistically significant.

Descriptive statistics				
Age category	**ROI**	**Sickle cell anemia, mean ± SD**	**Control, mean ± SD**	
ROI3	Study group	1	1.70	0.195
ROI3	Age category	1	1.38	0.243
ROI3	Study group × age category	1	0.81	0.370

Legend. SD, standard deviation; CI, confidence interval; FDR, false discovery rate; ROI, region of interest; SCA, sickle cell anemia. Pairwise comparisons were performed using Welch's t-test. For within-group comparisons, mean differences were calculated as the 18–29-year group minus the ≥ 30-year group; for between-group comparisons, differences were calculated as the SCA group minus the control group. P-values were adjusted for multiple comparisons using the Benjamini–Hochberg procedure. Hedges' g was used to estimate standardized effect sizes. Two-way ANOVA assessed the main effects of study group and age category and their interaction. All tests were two-sided; $p < 0.05$ in bold was considered statistically significant.

In ROI2, mean fractal dimension was lower in the SCA group than in controls among participants aged 18–29 years (1.2282 ± 0.0748 vs. 1.2975 ± 0.0885) and those aged ≥ 30 years (1.2688 ± 0.0923 vs. 1.3261 ± 0.0911). However, neither between-group comparison remained statistically significant after FDR adjustment (18–29 years: adjusted p = 0.058; ≥30 years: adjusted p = 0.054). Two-way ANOVA nevertheless showed a significant main effect of study group (F = 11.46, p = 0.001). The main effect of age category (p = 0.067) and the group-by-age interaction (p = 0.749) were not statistically significant (Table 4).

In ROI3, mean fractal dimension was similar between the SCA and control groups among participants aged 18–29 years (1.2531 ± 0.0884 vs. 1.2602 ± 0.1088). Among those aged ≥ 30 years, mean fractal dimension was lower in the SCA group than in controls (1.2579 ± 0.0669 vs. 1.2966 ± 0.0800). Although the unadjusted pairwise comparison indicated a difference (p = 0.037), it did not remain statistically significant after FDR adjustment (adjusted p = 0.089). Two-way ANOVA showed no significant main effect of study group (p = 0.195), age category (p = 0.243), or group-by-age interaction (p = 0.370) (Table 4).

3.5 Morphometric and Trabecular Connectivity Parameters

Morphometric and trabecular connectivity parameters were compared between the SCA and control groups according to age category and region of interest (Table 5). After adjustment for multiple comparisons using the Benjamini–Hochberg false discovery rate procedure, significant differences were observed predominantly among participants aged ≥ 30 years. The boxplots shown in Fig. 3 include only variables that remained statistically significant after FDR correction.

Table 5
Morphometric and trabecular connectivity parameters according to study group, age category, and region of interest.

Age category	ROI	Parameter	SCA (Mean ± SD)	Healthy Controls (Mean ± SD)	Raw *p*-value	FDR-adjusted *p*-value
18–29 years (n = 17/group)	ROI1	Trabecular area (mm²)	9.45 ± 1.73	10.60 ± 1.80	0.068	0.120
		Trabecular length (mm)	11.05 ± 4.57	13.44 ± 5.28	0.169	0.253
		Trabecular perimeter (mm)	25.88 ± 8.91	32.51 ± 12.38	0.084	0.140
		Endpoints (n)	11.88 ± 19.24	8.71 ± 5.34	0.835	0.835
		Junction pixels (n)	11.71 ± 8.12	24.59 ± 27.89	0.124	0.196
	ROI2	Trabecular area (mm²)	8.96 ± 1.64	9.28 ± 1.85	0.591	0.726
		Trabecular length (mm)	11.24 ± 2.39	12.92 ± 2.45	0.052	0.105
		Trabecular perimeter (mm)	27.38 ± 5.62	33.20 ± 7.43	**0.015**	**0.037**
		Endpoints (n)	8.35 ± 3.24	10.47 ± 6.04	**0.036**	0.540
		Junction pixels (n)	10.82 ± 4.03	17.29 ± 11.32	**0.016**	**0.037**
	ROI3	Trabecular area (mm²)	9.52 ± 1.28	9.59 ± 1.49	0.880	0.910
		Trabecular length (mm)	12.24 ± 2.81	12.29 ± 3.66	0.967	0.967
		Trabecular perimeter (mm)	29.62 ± 5.91	30.60 ± 5.92	0.631	0.726
		Endpoints (n)	9.76 ± 4.07	8.71 ± 4.28	0.564	0.696
		Junction pixels (n)	13.65 ± 7.25	14.53 ± 12.83	0.654	0.726
≥ 30 years (n = 33/group)	ROI1	Trabecular area (mm²)	10.11 ± 1.71	9.90 ± 1.72	0.635	0.726
		Trabecular length (mm)	11.26 ± 3.43	14.32 ± 4.19	**0.002**	**0.006**
		Trabecular perimeter (mm)	26.04 ± 7.75	35.14 ± 8.88	**< 0.001**	**< 0.001**
		Endpoints (n)	7.24 ± 3.46	11.94 ± 5.92	**< 0.001**	**0.002**
		Junction pixels (n)	10.09 ± 7.04	25.24 ± 16.76	**< 0.001**	**< 0.001**
	ROI2	Trabecular area (mm²)	9.21 ± 2.10	10.31 ± 1.45	**0.016**	**0.037**
		Trabecular length (mm)	12.22 ± 4.06	14.75 ± 3.30	**0.007**	**0.022**
		Trabecular perimeter (mm)	28.11 ± 7.34	34.70 ± 7.00	**< 0.001**	**0.002**
		Endpoints (n)	7.91 ± 3.25	9.58 ± 4.23	0.065	0.120
		Junction pixels (n)	13.82 ± 16.44	22.24 ± 11.32	**< 0.001**	**0.001**
	ROI3	Trabecular area (mm²)	9.38 ± 1.57	8.96 ± 1.70	**0.016**	**0.037**
		Trabecular length (mm)	12.11 ± 2.54	13.49 ± 2.96	**0.007**	**0.022**
		Trabecular perimeter (mm)	28.28 ± 4.90	33.51 ± 6.05	**< 0.001**	**0.002**
		Endpoints (n)	7.91 ± 3.91	11.33 ± 3.76	0.065	0.120
		Junction pixels (n)	11.27 ± 4.66	22.39 ± 16.47	**< 0.001**	**0.001**

Legend. SD, standard deviation; FDR, false discovery rate; ROI, region of interest; SCA, sickle cell anemia. Data are presented as mean ± SD. Between-group comparisons were performed using Welch's t-test for trabecular area, trabecular length, and trabecular perimeter, and the Mann–Whitney U test for endpoints and junction pixels. P-values were adjusted for multiple comparisons using the Benjamini–Hochberg procedure. Adjusted p-values (p-FDR) < 0.05 were considered statistically significant and are shown in bold.

Among participants aged 18–29 years, significant between-group differences were restricted to ROI2. The SCA group showed lower trabecular perimeter than controls (27.38 ± 5.62 mm vs. 33.20 ± 7.43 mm; p-FDR = 0.037) and lower junction pixel counts (10.82 ± 4.03 vs. 17.29 ± 11.32; p-FDR = 0.037). No other morphometric or connectivity parameter differed significantly between groups in this age category.

Among participants aged ≥ 30 years, differences were more extensive. In ROI1, the SCA group showed lower trabecular length (11.26 ± 3.43 mm vs. 14.32 ± 4.19 mm; p-FDR = 0.006), trabecular perimeter (26.04 ± 7.75 mm vs. 35.14 ± 8.88 mm; p-FDR < 0.001), endpoint counts (7.24 ± 3.46 vs. 11.94 ± 5.92; p-FDR = 0.002), and junction pixel counts (10.09 ± 7.04 vs. 25.24 ± 16.76; p-FDR < 0.001) compared with controls.

In ROI2, participants with SCA aged ≥ 30 years also exhibited lower trabecular area (9.21 ± 2.10 mm^2 vs. 10.31 ± 1.45 mm^2; p-FDR = 0.037), trabecular length (12.22 ± 4.06 mm vs. 14.75 ± 3.30 mm; p-FDR = 0.022), trabecular perimeter (28.11 ± 7.34 mm vs. 34.70 ± 7.00 mm; p-FDR = 0.002), and junction pixel counts (13.82 ± 16.44 vs. 22.24 ± 11.32; p-FDR = 0.001). Endpoint counts did not remain significantly different between groups after FDR correction.

In ROI3, significant differences among participants aged ≥ 30 years were observed for trabecular perimeter, endpoints, and junction pixels. The SCA group showed lower trabecular perimeter (28.28 ± 4.90 mm vs. 33.51 ± 6.05 mm; p-FDR = 0.002), fewer endpoints (7.91 ± 3.91 vs. 11.33 ± 3.76; p-FDR = 0.003), and fewer junction pixels (11.27 ± 4.66 vs. 22.39 ± 16.47; p-FDR = 0.002) than controls. Trabecular area and trabecular length were not significantly different between groups in this region.

Overall, the significant findings were concentrated mainly in participants aged ≥ 30 years and consistently indicated lower values in the SCA group, particularly for trabecular perimeter and connectivity-related parameters. The distribution of all comparisons that remained significant after FDR correction is illustrated in Fig. 3, in which the boxplots display the individual observations, medians, interquartile ranges, and mean values for the control and SCA groups.

3.6 Normalized Trabecular Microarchitecture in SCA and Healthy Controls

Normalized trabecular microarchitecture parameters were compared between the sickle cell anemia and control groups across the three regions of interest and two age categories (Table 6). Among participants aged 18–29 years, no statistically significant differences were observed between the SCA and healthy control groups for any normalized parameter across ROI1, ROI2, or ROI3 after Benjamini–Hochberg correction for multiple comparisons. Differences between groups were predominantly observed among participants aged ≥ 30 years (Table 6).

Table 6
Normalized trabecular microarchitecture in SCA and control groups by age and region.

Parameter	ROI	Age 18–29 years (n = 17): Mean difference (95% CI)	p-FDR	Age ≥ 30 years (n = 33): Mean difference (95% CI)	p-FDR
Trabecular area/total area (A/T)	ROI1	−0.075 (− 0.155 to 0.005)	0.196	0.013 (− 0.042 to 0.068)	0.761
	ROI2	−0.021 (− 0.101 to 0.058)	0.744	−0.072 (− 0.130 to − 0.014)	0.136
	ROI3	−0.005 (− 0.068 to 0.058)	0.951	0.027 (− 0.025 to 0.080)	0.531
Perimeter/total area (P/T)	ROI1	−0.433 (− 0.921 to 0.055)	0.220	**−0.594 (− 0.860 to − 0.327)**	**< 0.001**
	ROI2	−0.380 (− 0.678 to − 0.082)	0.136	**−0.430 (− 0.660 to − 0.201)**	**0.013**
	ROI3	−0.064 (− 0.332 to 0.203)	0.850	**−0.341 (− 0.518 to − 0.165)**	**0.007**
Perimeter/trabecular area (P/A)	ROI1	−0.384 (− 1.281 to 0.512)	0.575	**−0.995 (− 1.543 to − 0.447)**	**0.003**
	ROI2	−0.568 (− 1.263 to 0.127)	0.324	−0.244 (− 0.735 to 0.247)	0.617
	ROI3	−0.065 (− 0.642 to 0.511)	0.932	**−0.770 (− 1.278 to − 0.263)**	**0.033**
Length/trabecular area (L/A)	ROI1	−0.135 (− 0.550 to 0.280)	0.653	**−0.340 (− 0.567 to − 0.113)**	**0.019**
	ROI2	−0.138 (− 0.378 to 0.102)	0.552	−0.089 (− 0.289 to 0.111)	0.654
	ROI3	−0.006 (− 0.277 to 0.264)	0.986	−0.196 (− 0.374 to − 0.018)	0.135
Length/total area (L/T)	ROI1	−0.156 (− 0.379 to 0.068)	0.385	**−0.200 (− 0.323 to − 0.078)**	**0.008**
	ROI2	−0.109 (− 0.219 to 0.000)	0.228	−0.165 (− 0.284 to − 0.047)	0.117
	ROI3	−0.003 (− 0.151 to 0.145)	0.986	−0.090 (− 0.178 to − 0.002)	0.170
Endpoints/total area (E/T)	ROI1	0.207 (− 0.431 to 0.846)	0.653	**−0.307 (− 0.462 to − 0.151)**	**0.001**
	ROI2	−0.138 (− 0.358 to 0.081)	0.517	−0.109 (− 0.229 to 0.012)	0.274
	ROI3	0.069 (− 0.120 to 0.258)	0.663	**−0.224 (− 0.346 to − 0.101)**	**0.007**
Endpoints/length (E/L)	ROI1	0.425 (− 0.317 to 1.167)	0.479	−0.173 (− 0.348 to 0.001)	0.196
	ROI2	−0.065 (− 0.364 to 0.235)	0.785	0.017 (− 0.147 to 0.181)	0.871
	ROI3	0.058 (− 0.258 to 0.375)	0.931	−0.240 (− 0.432 to − 0.049)	0.086
Endpoints/perimeter (E/P)	ROI1	0.186 (− 0.131 to 0.504)	0.479	−0.048 (− 0.112 to 0.015)	0.316
	ROI2	0.007 (− 0.088 to 0.102)	0.885	0.019 (− 0.039 to 0.076)	0.710
	ROI3	0.049 (− 0.037 to 0.135)	0.487	−0.065 (− 0.125 to − 0.006)	0.135
Endpoints/trabecular area (E/A)	ROI1	0.363 (− 0.544 to 1.271)	0.591	**−0.540 (− 0.855 to − 0.225)**	**0.005**
	ROI2	−0.202 (− 0.683 to 0.279)	0.658	−0.020 (− 0.274 to 0.235)	0.885
	ROI3	0.122 (− 0.231 to 0.476)	0.680	**−0.463 (− 0.792 to − 0.134)**	**0.041**
Junction pixels/total area (J/T)	ROI1	−0.841 (− 1.770 to 0.088)	0.213	**−0.989 (− 1.400 to − 0.578)**	**< 0.001**
	ROI2	−0.422 (− 0.807 to − 0.038)	0.194	−0.550 (− 1.001 to − 0.099)	0.136
	ROI3	−0.058 (− 0.529 to 0.414)	0.932	**−0.726 (− 1.113 to − 0.339)**	**0.007**
Junction pixels/length (J/L)	ROI1	−0.565 (− 1.162 to 0.031)	0.196	**−0.779 (− 1.085 to − 0.474)**	**< 0.001**
	ROI2	−0.368 (− 0.762 to 0.025)	0.265	−0.449 (− 0.749 to − 0.149)	0.095
	ROI3	0.013 (− 0.479 to 0.505)	0.986	**−0.726 (− 1.233 to − 0.218)**	**0.041**
Junction pixels/perimeter (J/P)	ROI1	−0.224 (− 0.483 to 0.036)	0.223	**−0.300 (− 0.436 to − 0.165)**	**< 0.001**
	ROI2	−0.111 (− 0.257 to 0.036)	0.386	−0.193 (− 0.347 to − 0.039)	0.136
	ROI3	0.000 (− 0.205 to 0.205)	1.000	**−0.241 (− 0.385 to − 0.096)**	**0.015**
Junction pixels/trabecular area (J/A)	ROI1	−1.154 (− 2.490 to 0.183)	0.223	**−1.508 (− 2.098 to − 0.919)**	**< 0.001**

Legend: Comparisons between the sickle cell anemia (SCA) and control groups were performed using Welch's t-test for independent samples. Data are presented as mean differences (95% confidence intervals [CI]), calculated as SCA minus control; negative values indicate lower parameter values in the SCA group. P-values were adjusted using the Benjamini–Hochberg procedure to control the false discovery rate (FDR). Adjusted p-values (p-FDR) < 0.05 were considered statistically significant and are shown in bold. A, trabecular area; T, total area; P, trabecular perimeter; L, trabecular length; E, endpoints; J, junction pixels; ROI, region of interest; CI, confidence interval; FDR, false discovery rate.

Parameter	ROI	Age 18–29 years (n = 17): Mean difference (95% CI)	p-FDR	Age ≥ 30 years (n = 33): Mean difference (95% CI)	p-FDR
	ROI2	−0.660 (− 1.329 to 0.009)	0.228	−0.656 (− 1.297 to − 0.015)	0.228
	ROI3	−0.095 (− 0.931 to 0.740)	0.932	**−1.396 (− 2.343 to − 0.449)**	**0.036**
Junction pixels/endpoints (J/E)	ROI1	−1.494 (− 3.076 to 0.087)	0.196	**−0.904 (− 1.540 to − 0.269)**	**0.027**
	ROI2	−0.487 (− 1.082 to 0.109)	0.324	−0.939 (− 1.984 to 0.106)	0.274
	ROI3	−0.372 (− 1.143 to 0.400)	0.564	−0.221 (− 0.779 to 0.337)	0.629

Legend: Comparisons between the sickle cell anemia (SCA) and control groups were performed using Welch's t-test for independent samples. Data are presented as mean differences (95% confidence intervals [CI]), calculated as SCA minus control; negative values indicate lower parameter values in the SCA group. P-values were adjusted using the Benjamini–Hochberg procedure to control the false discovery rate (FDR). Adjusted p-values (p-FDR) < 0.05 were considered statistically significant and are shown in bold. A, trabecular area; T, total area; P, trabecular perimeter; L, trabecular length; E, endpoints; J, junction pixels; ROI, region of interest; CI, confidence interval; FDR, false discovery rate.

Among participants aged 18–29 years, effect sizes were generally small to moderate, and no comparisons remained statistically significant after false discovery rate (FDR) correction. In contrast, among participants aged ≥ 30 years, negative Hedges' g values predominated, particularly in ROI1 and ROI3, indicating lower normalized parameter values in the SCA group than in controls. The most consistent differences involved trabecular perimeter-related measures and, particularly, junction pixels (Table 6).

In ROI1, participants aged ≥ 30 years with SCA had significantly lower values for total perimeter-to-area ratio (mean difference = − 0.594; 95% CI, − 0.860 to − 0.327; p-FDR < 0.001), trabecular perimeter-to-area ratio (mean difference = − 0.995; 95% CI, − 1.543 to − 0.447; p-FDR = 0.003), trabecular length-to-area ratio (mean difference = − 0.340; 95% CI, − 0.567 to − 0.113; p-FDR = 0.019), and total length-to-area ratio (mean difference = − 0.200; 95% CI, − 0.323 to − 0.078; p-FDR = 0.008). The trabecular area-to-total area ratio did not differ significantly between groups. The SCA group also showed lower endpoint-to-total area ratios (mean difference = − 0.307; 95% CI, − 0.462 to − 0.151; p-FDR = 0.001) and endpoint-to-trabecular area ratios (mean difference = − 0.540; 95% CI, − 0.855 to − 0.225; p-FDR = 0.005). Endpoint-to-length and endpoint-to-perimeter ratios were not significantly different after FDR correction (Table 6).

The most consistent differences in ROI1 involved junction pixel parameters. Among participants aged ≥ 30 years, the SCA group had lower junction pixel-to-total area ratios (mean difference = − 0.989; 95% CI, − 1.400 to − 0.578; p-FDR < 0.001), junction pixel-to-length ratios (mean difference = − 0.779; 95% CI, − 1.085 to − 0.474; p-FDR < 0.001), junction pixel-to-perimeter ratios (mean difference = − 0.300; 95% CI, − 0.436 to − 0.165; p-FDR < 0.001), junction pixel-to-trabecular area ratios (mean difference = − 1.508; 95% CI, − 2.098 to − 0.919; p-FDR < 0.001), and junction pixel-to-endpoint ratios (mean difference = − 0.904; 95% CI, − 1.540 to − 0.269; p-FDR = 0.027) (Table 6).

In ROI2, differences were less pronounced. After FDR correction, only the total perimeter-to-area ratio remained significantly lower in the SCA group among participants aged ≥ 30 years (mean difference = − 0.430; 95% CI, − 0.660 to − 0.201; p-FDR = 0.013). The other normalized parameters involving area, length, endpoints, and junction pixels did not differ significantly after correction (Table 6).

In ROI3, significant differences were also restricted to participants aged ≥ 30 years. The SCA group had lower total perimeter-to-area ratios (mean difference = − 0.341; 95% CI, − 0.518 to − 0.165; p-FDR = 0.007) and trabecular perimeter-to-area ratios (mean difference = − 0.770; 95% CI, − 1.278 to − 0.263; p-FDR = 0.033). No significant differences were observed for the trabecular area-to-total area, trabecular length-to-area, or total length-to-area ratios. For endpoint-related parameters in ROI3, the SCA group had lower endpoint-to-total area ratios (mean difference = − 0.224; 95% CI, − 0.346 to − 0.101; p-FDR = 0.007) and endpoint-to-trabecular area ratios (mean difference = − 0.463; 95% CI, − 0.792 to − 0.134; p-FDR = 0.041). Endpoint-to-length and endpoint-to-perimeter ratios were not significantly different after FDR correction (Table 6).

Junction pixel-related parameters were also lower in the SCA group in ROI3 among participants aged ≥ 30 years. Significant differences were observed for junction pixel-to-total area ratios (mean difference = − 0.726; 95% CI, − 1.113 to − 0.339; p-FDR = 0.007), junction pixel-to-length ratios (mean difference = − 0.726; 95% CI, − 1.233 to − 0.218; p-FDR = 0.041), junction pixel-to-perimeter ratios (mean difference = − 0.241; 95% CI, − 0.385 to − 0.096; p-FDR = 0.015), and junction pixel-to-trabecular area ratios (mean difference = − 1.396; 95% CI, − 2.343 to − 0.449; p-FDR = 0.036). The junction pixel-to-endpoint ratio did not differ significantly between groups (Table 6).

3.7 Correlations Between Laboratory Markers and Mandibular Radiographic Parameters in Patients with Sickle Cell Anemia and Healthy Controls, Stratified by Age Group

Correlations between laboratory markers and radiographic mandibular parameters were assessed using Spearman's rank correlation coefficient, with analyses stratified by age group (18–29 and ≥ 30 years) when applicable (Table 7 and Supplementary Files 1 to 4). The radiographic variables included mean pixel intensity, fractal dimension, lacunarity, trabecular area-to-total area ratio (A/T), and total skeleton length-to-total area ratio (L/T), evaluated across ROI1, ROI2, and ROI3. Here, P-values were adjusted using the Benjamini–Hochberg procedure to account for multiple comparisons within each family of analyses.

Table 7
Correlations of hemoglobin and HbF with radiographic parameters in SCA by age group.

ROI	Variable	Hemoglobin			Hemoglobin			HbF			HbF		
		18–29 years (n = 17)	p	p-FDR	≥ 30 years (n = 33)	p	p-FDR	18–29 years (n = 17)	p	p-FDR	≥ 30 years (n = 33)	p	p-FDR
		ρ Spearman			ρ Spearman			ρ Spearman			ρ Spearman		
ROI1	Mean pixel intensity	0.525	0.030	0.228	0.135	0.453	0.764	−0.221	0.395	0.740	−0.132	0.464	0.810
ROI1	Fractal dimension	0.064	0.808	0.865	0.007	0.971	0.971	−0.140	0.593	0.918	0.192	0.284	0.810
ROI1	Lacunarity	0.308	0.229	0.491	−0.096	0.596	0.893	−0.113	0.667	0.918	0.079	0.664	0.819
ROI1	A/T	−0.076	0.772	0.865	−0.061	0.736	0.954	0.262	0.309	0.663	−0.026	0.885	0.885
ROI1	L/T	0.382	0.130	0.400	0.055	0.763	0.954	−0.013	0.959	0.978	0.150	0.404	0.810
ROI2	Mean pixel intensity	0.091	0.729	0.865	−0.281	0.114	0.609	0.289	0.260	0.663	0.052	0.774	0.829
ROI2	Fractal dimension	0.247	0.338	0.564	−0.204	0.255	0.761	0.298	0.245	0.663	0.231	0.195	0.732
ROI2	Lacunarity	0.310	0.225	0.491	0.275	0.122	0.609	0.047	0.859	0.978	−0.067	0.709	0.819
ROI2	A/T	−0.004	0.989	0.989	−0.134	0.459	0.764	0.110	0.673	0.918	−0.123	0.496	0.810
ROI2	L/T	0.100	0.704	0.865	−0.165	0.359	0.764	0.280	0.276	0.663	0.163	0.365	0.810
ROI3	Mean pixel intensity	0.566	0.018	0.228	0.184	0.304	0.761	−0.017	0.948	0.978	0.086	0.632	0.819
ROI3	Fractal dimension	−0.379	0.133	0.400	−0.224	0.210	0.761	0.436	0.080	0.642	0.239	0.180	0.732
ROI3	Lacunarity	0.071	0.786	0.865	−0.038	0.832	0.960	−0.309	0.228	0.663	0.239	0.181	0.732
ROI3	A/T	−0.275	0.286	0.536	0.017	0.926	0.971	0.007	0.978	0.978	−0.111	0.540	0.810
ROI3	L/T	−0.448	0.071	0.356	−0.301	0.089	0.609	0.429	0.086	0.642	0.251	0.159	0.732

Legend. ρ = Spearman's rank correlation coefficient; HbF = fetal hemoglobin; MPI = mean pixel intensity; A/T = trabecular area-to-total area ratio; L/T = total skeleton length-to-total area ratio; p-FDR = p-value adjusted using the Benjamini–Hochberg procedure. Nominal associations were defined as unadjusted p-values < 0.05. No association remained statistically significant after FDR correction.

Initially, among participants aged 18–29 years, total hemoglobin showed moderate positive correlations with mean pixel intensity in ROI1 (ρ Spearman = 0.525; p = 0.030) and ROI3 (ρ Spearman = 0.566; p = 0.018) (Table 7). However, neither association remained statistically significant after adjustment for multiple comparisons (p-FDR = 0.228 for both) (Table 7). Among participants aged ≥ 30 years, no statistically significant correlations were observed between total hemoglobin and any radiographic parameter, even before adjustment. No correlations between fetal hemoglobin (HbF) and radiographic parameters reached nominal statistical significance in either age group (Table 7). In participants aged 18–29 years, HbF showed moderate positive correlations with fractal dimension (ρ Spearman = 0.436; p = 0.080) and L/T (ρ Spearman = 0.429; p = 0.086) in ROI3. Positive but weaker correlations were observed in the ≥ 30-year group for fractal dimension (ρ Spearman = 0.239; p = 0.180) and L/T (ρ Spearman = 0.251; p = 0.159) in the same region (Table 7). These findings did not provide statistically significant evidence of associations after adjustment for multiple comparisons (Table 7).

According to hemolysis index, the principal component analysis showed satisfactory sampling adequacy (Kaiser–Meyer–Olkin index = 0.789), and Bartlett's test of sphericity was statistically significant ($\chi^2 = 65.54$, df = 6; $p < 0.001$). The first principal component had an eigenvalue of 2.584 and explained 64.6% of the total variance in the hemolysis markers. All markers loaded positively on this component: lactate dehydrogenase (LDH), 0.855; aspartate aminotransferase (AST), 0.722; total bilirubin, 0.855; and reticulocyte count, 0.776. LDH and total bilirubin each contributed 28.3% to the component, followed by reticulocytes (23.3%) and AST (20.1%). The hemolysis index had a median of 0.074 (interquartile range [IQR], − 0.821 to 0.701) and ranged from − 2.055 to 2.080. Its distribution did not significantly deviate from normality according to the Shapiro–Wilk test (p = 0.764). No significant difference in the index was observed between the two age groups (Mann–Whitney U test, p = 0.526).

In the overall sample, no statistically significant correlations were identified between the hemolysis index and the radiographic parameters after adjustment for multiple comparisons (Supplementary Files 1). The largest coefficients were observed in ROI3, where the index was positively correlated with L/T (ρ Spearman = 0.274; p = 0.054; p-FDR = 0.441) and fractal dimension (ρ Spearman = 0.245; p = 0.086; p-FDR = 0.441). A negative correlation with lacunarity was observed in ROI2 (ρ Spearman = − 0.244; p = 0.088; p-FDR = 0.441). In the 18–29-year group, the largest coefficient was a positive

correlation between the hemolysis index and L/T in ROI3 (ρ Spearman = 0.452; p = 0.068; p-FDR = 0.518). Among participants aged ≥ 30 years, the hemolysis index was negatively correlated with lacunarity in ROI2 (ρ Spearman = − 0.442; p = 0.010), but this association did not remain statistically significant after adjustment (p-FDR = 0.150). No other significant associations were identified (Supplementary Files 1).

In relation to iron metabolism markers (Supplementary Files 2), ferritin showed no correlations with $p < 0.05$ in either age group. In the overall sample, transferrin saturation showed nominal positive correlations with fractal dimension in ROI3 (ρ Spearman = 0.352; p = 0.012; p-FDR = 0.115) and with L/T in the same region (ρ Spearman = 0.341; p = 0.015; p-FDR = 0.115). Neither association remained statistically significant after adjustment. No nominally significant correlations were observed in participants aged 18–29 years. Among those aged ≥ 30 years, transferrin saturation was positively correlated with fractal dimension (ρ Spearman = 0.415; p = 0.016; p-FDR = 0.133) and L/T (ρ Spearman = 0.410; p = 0.018; p-FDR = 0.133) in ROI3. These associations also did not remain significant after correction for multiple comparisons (Supplementary Files 2).

Among participants aged 18–29 years, alkaline phosphatase showed nominal positive correlations with mean pixel intensity in ROI2 (ρ Spearman = 0.574; p = 0.016; p-FDR = 0.210) and with A/T in ROI1 (ρ Spearman = 0.532; p = 0.028; p-FDR = 0.210) (Supplementary Files 3). A further positive correlation with A/T in ROI2 was observed (ρ Spearman = 0.426; p = 0.088; p-FDR = 0.439), although it did not reach nominal statistical significance (Supplementary Files 3). None of these associations remained statistically significant after adjustment for multiple comparisons. Among participants aged ≥ 30 years, no correlations reached nominal statistical significance. The largest coefficient was a negative correlation between alkaline phosphatase and lacunarity in ROI2 (ρ Spearman = − 0.332; p = 0.059; p-FDR = 0.882) (Supplementary Files 3).

Accordingly to total leukocyte and neutrophil counts, among participants aged 18–29 years, no statistically significant correlations were observed between total leukocyte count and the radiographic parameters (Supplementary Files 4). The largest coefficients were negative correlations with fractal dimension in ROI2 (ρ Spearman = − 0.349; p = 0.169; p-FDR = 0.852) and ROI3 (ρ Spearman = − 0.346; p = 0.174; p-FDR = 0.852), and with L/T in ROI1 (ρ Spearman = − 0.332; p = 0.193; p-FDR = 0.852). Among participants aged ≥ 30 years, no statistically significant correlations were identified. The largest coefficient was a negative correlation between total leukocyte count and lacunarity in ROI2 (ρ = −0.270; p = 0.129; p-FDR = 0.870). Negative correlations were also observed with lacunarity (ρ = −0.201; p = 0.261), fractal dimension (ρ Spearman = − 0.148; p = 0.410), and L/T (ρ = −0.136; p = 0.450) in ROI3; all had p-FDR = 0.870 (Supplementary Files 4).

4. Discussion

Sickle cell anemia is associated with systemic mechanisms that may affect bone metabolism and trabecular organization, including chronic hemolysis, compensatory bone marrow expansion, recurrent hypoxia, vaso-occlusion, and altered bone remodeling [4, 22]. In this study, quantitative panoramic radiographic analysis revealed differences in mandibular trabecular bone characteristics between patients with SCA and healthy controls (HC), particularly in mean pixel intensity, fractal dimension, and normalized morphometric parameters. These differences varied according to mandibular region and age group, indicating that the radiographic manifestations of bone involvement in SCA may not be uniform. Because pixel intensity, fractal dimension, lacunarity, and morphometric parameters represent distinct properties of radiographically projected bone structure, their combined assessment provides a more comprehensive characterization of trabecular organization. Accordingly, integrating these variables allows changes in radiopacity, complexity, spatial heterogeneity, and connectivity to be considered within a common structural framework, rather than interpreting trabecular alterations based on a single indicator [13, 14].

4.1 Demographic characteristics

The study population had a median age of 32.5 years, with a predominance of female participants (68%). This demographic profile was similar to that reported by Almeida et al., who investigated mandibular bone microstructure in 57 individuals with sickle cell disease and 57 controls, although their sample showed a more balanced sex distribution [23]. Previous radiographic investigations have included younger populations and different age distributions, which may contribute to variations in the mandibular findings reported in the literature [12, 24].

An important methodological characteristic of the present study was individual matching by age and sex between the SCA and HC groups. This approach minimized differences in these demographic characteristics between groups, facilitating the interpretation of radiographic comparisons. Nevertheless, age remains relevant to mandibular bone organization, particularly because skeletal alterations associated with SCA may develop throughout adulthood.

4.2 Mean pixel intensity

Mean pixel intensity differed according to mandibular region and age group. The most pronounced difference occurred in the mandibular ramus (ROI1), where patients with SCA aged 18–29 years showed significantly lower values than HC participants. Similar reductions in radiographic pixel intensity have been described in conditions associated with altered mandibular bone structure, including osteoporosis and radiotherapy-related bone changes [25–28]. Studies combining histogram analysis with other quantitative imaging methods also support the potential usefulness of grayscale measurements for characterizing radiographic bone patterns [29].

The lower pixel intensity observed in ROI1 may reflect changes in the radiographic distribution of mineralized trabecular structures and medullary spaces. In SCA, chronic anemia and increased erythropoietic demand may stimulate bone marrow expansion, while recurrent hypoxia and altered bone remodeling may contribute to changes in trabecular organization [4, 22]. However, pixel intensity is influenced by radiographic acquisition, image processing, and projection geometry and should not be interpreted as a direct measurement of bone mineral density [25, 29, 30].

The absence of consistent differences in the remaining mandibular regions suggests that radiographic changes associated with SCA may depend on the anatomical region evaluated. Variations in trabecular arrangement, local functional loading, and projected bone thickness may contribute to this heterogeneity. These factors may partially explain why ROI1 showed greater sensitivity in detecting radiographic differences between the study groups.

4.3 Lacunarity

Lacunarity provides information about the spatial distribution of gaps and heterogeneity within the trabecular pattern. Two structures may exhibit similar fractal dimensions while presenting different spatial arrangements of trabeculae and medullary spaces. Previous dental radiographic studies have demonstrated the applicability of lacunarity in characterizing bone texture [13, 31].

In the present study, no between-group differences in lacunarity remained statistically significant after correction for multiple comparisons. However, a group-by-age interaction was identified in the molar region (ROI2), suggesting that the relationship between SCA and lacunarity differed across age categories. This finding indicates a potentially localized pattern of age-dependent variation in trabecular spatial organization, although the absence of significant adjusted pairwise comparisons requires cautious interpretation.

These findings may be explained by the multifactorial effects of SCA on mandibular bone. Bone marrow expansion, vaso-occlusive events, and altered bone remodeling may influence trabecular organization differently across anatomical regions and stages of skeletal maturity [4, 22]. Moreover, lacunarity depends on image segmentation, the definition of foreground structures, and the scale of analysis, all of which may influence the magnitude and direction of the resulting values [13, 31].

Although lacunarity exhibited variation related to the interaction between study group and age category in ROI2, the results did not demonstrate a sufficiently consistent pattern to distinguish patients with SCA from HC participants after statistical correction.

4.4 Fractal dimension

Fractal dimension was one of the most consistent radiographic parameters differentiating patients with SCA from healthy controls. Significantly lower values were observed in ROI1 in both age groups, suggesting reduced complexity of the projected mandibular trabecular pattern. These findings are consistent with those reported by Demirbaş et al., who identified lower mandibular fractal dimension in patients with SCA, particularly among younger individuals [12].

Regional differences in fractal dimension have also been described in children and adolescents with sickle cell disease. Temur et al. identified changes in fractal dimension and radiomorphometric parameters in selected mandibular regions, indicating that skeletal alterations may occur before adulthood and may not uniformly affect the entire mandible [32].

However, findings in the literature are not entirely consistent. Serindere and Belgin reported no significant differences in mandibular fractal dimension between patients with hemoglobinopathies and controls [33]. These discrepancies may reflect differences in participant characteristics, age, genotype, ROI location and size, radiographic equipment, and image-processing procedures. A recent systematic review also highlighted considerable methodological heterogeneity and limited certainty of evidence regarding mandibular radiographic alterations in sickle cell disease [15].

The biological plausibility of reduced fractal complexity is supported by the effects of chronic hemolytic anemia, compensatory bone marrow hyperplasia, hypoxia, and inflammation-associated bone remodeling. These mechanisms may alter the spatial arrangement of trabeculae and contribute to a less complex radiographic pattern [4, 22]. Furthermore, three-dimensional imaging studies have demonstrated reduced trabecular number and thickness, increased trabecular separation, and greater mandibular bone porosity in individuals with sickle cell disease [23]. Although tomographic microstructural measurements and fractal dimension obtained from panoramic radiographs are not directly equivalent, these findings support a convergent interpretation of altered mandibular trabecular organization.

The absence of a significant group-by-age interaction for fractal dimension indicates that the effect of SCA did not differ statistically between the two age categories, despite significant stratified comparisons in ROI1. Therefore, age-related differences should not be interpreted as evidence of progressive deterioration in fractal complexity. Importantly, fractal dimension reflects the complexity of a two-dimensional radiographic projection and cannot directly determine bone mineral density, mechanical strength, or fracture risk [15].

4.5 Trabecular morphometric and connectivity parameters

Complementary morphometric analysis provided information on the extent and organization of the mandibular trabecular network through measurements of area, perimeter, length, terminal points, and junction pixels. The application of these measurements is consistent with previous quantitative radiographic approaches, particularly those described by de Sá Cavalcante et al. [14].

In the present study, the most pronounced differences in normalized morphometric parameters occurred among participants aged ≥ 30 years, particularly in ROI1 and ROI3. Reductions in perimeter- and length-related measurements suggest alterations in the extent and distribution of the projected trabecular network. A reduced perimeter relative to trabecular area or total ROI area may indicate a less finely subdivided network, characterized by changes in trabecular contours and spatial distribution [14, 23].

Changes in terminal points and junction pixels provided information about the arrangement of trabecular branches. Reduced junction-related measurements may reflect fewer branching elements and simplification of the projected trabecular network. A reduction in terminal points may coexist with shorter trabeculae and fewer branches, indicating modifications in the spatial organization and extent of the trabecular network [14].

These results are consistent with tomographic evidence of reduced trabecular number, increased trabecular separation, and greater bone porosity in sickle cell disease [23]. They are also consistent with the understanding that skeletal involvement in SCA includes alterations in bone quality and architecture that are not necessarily explained by bone mineral density alone [34, 35].

The predominance of morphometric differences among participants aged ≥ 30 years may reflect the cumulative influence of chronic anemia, bone marrow expansion, vaso-occlusion, and altered bone remodeling. Experimental and clinical studies have described mechanisms linking SCA to bone inflammation, osteoclast activity, chronic pain, and age-associated skeletal complications [22, 36, 37]. However, the cross-sectional design does not allow these findings to be interpreted as evidence of progressive bone deterioration with aging.

The absence of significant differences in normalized morphometric parameters among younger adults does not exclude early skeletal involvement, as previous studies have demonstrated mandibular radiographic abnormalities in children and adolescents with sickle cell disease [32]. These results suggest that radiographic manifestations of bone involvement may exhibit distinct characteristics according to age group and the mandibular region evaluated.

Normalization of morphometric measurements allowed trabecular characteristics to be compared relative to total ROI area or other structural measures, helping distinguish differences in network organization from variations in absolute measurements. This approach has previously been applied in quantitative mandibular bone texture analysis [14]. Systematic evaluations of mandibular radiomorphometric parameters also emphasize the importance of methodological standardization and the limitations of indirect radiographic indicators of skeletal status [15, 38].

Taken together, the morphometric findings suggest that SCA is associated with a less extensive and less interconnected projected trabecular network in selected mandibular regions, particularly among older adults. Changes in perimeter, length, and junction-related parameters indicate a possible simplification of trabecular organization in these regions.

4.7 Associations between hematological, biochemical, and mandibular radiographic parameters

The exploratory analysis of hematological and biochemical markers investigated whether systemic characteristics of SCA were associated with mandibular radiographic parameters. Although some nominally significant correlations were identified, none remained statistically significant after Benjamini–Hochberg correction. Consequently, these associations should be interpreted as exploratory findings rather than confirmed relationships.

Hemoglobin concentration showed nominally significant positive correlations with mean pixel intensity in selected regions among younger participants, whereas fetal hemoglobin (HbF) showed positive but nonsignificant relationships with fractal dimension and relative trabecular length in ROI3. These findings are biologically plausible because higher HbF concentrations inhibit HbS polymerization and may reduce hemolysis and vaso-occlusive complications [7, 8]. Previous investigations have also associated lower HbF concentrations with reduced bone mineral density or more severe skeletal manifestations in sickle cell disease [35, 39].

The composite hemolysis index showed a nominally significant negative correlation with lacunarity in ROI2 among participants aged ≥ 30 years, but this association did not remain significant after statistical adjustment. Chronic hemolysis has been associated with impaired bone health, and previous investigations have linked hemolytic activity to reduced bone mass and other clinical manifestations of SCA [8, 40, 41]. However, interpretation of this correlation is conditioned by the characteristics of lacunarity, whose magnitude depends on the spatial distribution of the structures considered in the analysis.

Regarding iron metabolism, ferritin showed no significant association with mandibular radiographic parameters after adjustment. This finding should be interpreted considering that serum ferritin is influenced by inflammation and does not directly quantify tissue iron overload. Previous studies have reported inconsistent relationships between iron overload and skeletal abnormalities in SCA, while its assessment may require more specific methods [9, 42, 43].

Transferrin saturation showed nominally significant associations with fractal dimension and relative trabecular length in ROI3, suggesting a possible relationship between iron metabolism and local trabecular organization. However, these associations did not remain significant after statistical correction. This uncertainty is consistent with evidence that bone abnormalities and fracture risk in SCA cannot be explained exclusively by changes in mineral density or iron-related laboratory markers [44].

Alkaline phosphatase showed nominally significant positive associations with selected radiographic parameters, particularly among participants aged 18–29 years. These findings may reflect changes in bone remodeling; however, total alkaline phosphatase is not bone-specific and may also be influenced by hepatobiliary processes. Studies investigating bone turnover markers in SCA have described abnormalities in osteoblastic and osteoclastic activity, supporting the biological relevance of this analysis without establishing a direct association with mandibular trabecular parameters [9, 45].

Total leukocyte count showed no significant correlations with radiographic parameters. Although chronic inflammation contributes to the pathophysiology of sickle cell bone disease, peripheral leukocyte count is a nonspecific indicator and may not adequately represent the local inflammatory mechanisms affecting bone remodeling [22, 36, 46].

Overall, the absence of significant correlations after statistical adjustment suggests that individual laboratory markers did not independently explain the mandibular radiographic variations observed in this sample. Bone involvement in SCA is likely multifactorial, with anemia, hemolysis, bone marrow

expansion, inflammation, iron metabolism, and altered bone remodeling potentially contributing through interconnected mechanisms [5, 22, 23]. Larger studies integrating radiographic, clinical, and laboratory measurements are needed to clarify these relationships.

4.8 Study limitations and clinical implications

Several limitations should be considered. First, the cross-sectional design prevents causal inference and does not establish whether radiographic differences progress with age. Furthermore, although participants were individually matched by age and sex, residual confounding by clinical severity, treatment exposure, nutritional status, and other factors affecting bone metabolism cannot be excluded.

Another important limitation concerns the use of panoramic radiographs, which provide two-dimensional representations of trabecular structures and are influenced by projection geometry, acquisition conditions, and image processing. Consequently, the assessed parameters should not be considered direct measurements of three-dimensional microarchitecture, bone mineral density, or mechanical strength. The use of standardized ROIs and consistent processing procedures improves within-study comparability but does not eliminate these methodological limitations [15].

Despite these limitations, quantitative panoramic radiographic analysis identified regional differences in mandibular trabecular organization associated with SCA. These findings broaden the understanding of maxillofacial skeletal manifestations of the disease and may contribute to future investigations of radiographic parameters potentially applicable to the dental assessment of these patients, although their diagnostic and clinical utility requires further validation.

5. Conclusion

Sickle cell anemia was associated with region-specific alterations in mandibular trabecular bone, characterized by reduced pixel intensity and fractal complexity, particularly in the mandibular ramus, as well as changes in trabecular organization and connectivity, mainly among individuals aged 30 years or older. These radiographic alterations varied according to anatomical region and age group, with no significant associations with hematological or biochemical markers among patients with sickle cell anemia. Quantitative panoramic radiographic analysis may provide complementary information on mandibular bone involvement in sickle cell anemia, although further studies are needed to establish its clinical applicability.

Abbreviations

ANOVA
Analysis of variance
AST
Aspartate aminotransferase
CAAE
Certificate of Presentation for Ethical Consideration
CAPES
Coordination for the Improvement of Higher Education Personnel
CI
Confidence interval
CNPq
National Council for Scientific and Technological Development
FD
Fractal dimension
FDR
False discovery rate
FUNCAP
Ceará Foundation for Scientific and Technological Development Support
HbF
Fetal hemoglobin
HbS
Hemoglobin S
HBB
Beta-globin gene
HC
Healthy controls
HEMOCE
Hematology and Hemotherapy Center of Ceará
IQR
Interquartile range
LDH
Lactate dehydrogenase

LPHGDH
Hemoglobinopathies and Genetics of Hematological Diseases Research Laboratory
MPI
Mean pixel intensity
p-FDR
False discovery rate-adjusted p value
ROI
Region of interest
SCA
Sickle cell anemia
SD
Standard deviation
TIFF
Tagged Image File Format

Declarations

Ethics approval and consent to participate

The study was conducted in accordance with the Declaration of Helsinki and was approved by the Research Ethics Committee of the Hematology and Hemotherapy Center of Ceará (HEMOCE), Brazil (CAAE No. 81791424.7.0000.8152). Written informed consent to participate was obtained from all participants.

Consent for publication

Written informed consent for publication of the anonymized radiographic image was obtained from the participant.

Author Contribution

D T O C, H L R J, A C C, F W G C, L R C, A E M, S M C D and R P G L contributed to the conception of the study and to writing the manuscript. All authors read and approved the final manuscript.

Acknowledgement

The authors acknowledge the Ceará Foundation for the Support of Scientific and Technological Development (FUNCAP) for its financial support.

Availability of data and materials

The datasets generated and/or analysed during the current study are not publicly available because they contain clinical and radiographic data from human participants but are available from the corresponding author on reasonable request and subject to applicable ethical and data-protection requirements.

Competing interests

The authors declare that they have no competing interests.

Funding

This study was funded in part by the Coordination for the Improvement of Higher Education Personnel - Brazil (CAPES), Finance Code 001, through a doctoral fellowship awarded to Diego Thiers Oliveira Carneiro, and by the Ceará Foundation for Scientific and Technological Development Support (FUNCAP; grant ITR-00214-00056.01.00/23).

The funding agencies had no role in the design of the study; data collection, analysis, or interpretation; writing of the manuscript; or the decision to submit the manuscript for publication.

References

1. Kato GJ, Piel FB, Reid CD, Gaston MH, Ohene-Frempong K, Krishnamurti L, et al. Sickle cell disease. Nat Rev Dis Primers. 2018;4:18010. https://doi.org/10.1038/nrdp.2018.10.
2. Sundd P, Gladwin MT, Novelli EM. Pathophysiology of sickle cell disease. Annu Rev Pathol. 2019;14:263–92. https://doi.org/10.1146/annurev-pathmechdis-012418-012838.

3. Kato GJ, Steinberg MH, Gladwin MT. Intravascular hemolysis and the pathophysiology of sickle cell disease. J Clin Invest. 2017;127(3):750–60. https://doi.org/10.1172/JCI89741.
4. Almeida A, Roberts I. Bone involvement in sickle cell disease. Br J Haematol. 2005;129(4):482–90. https://doi.org/10.1111/j.1365-2141.2005.05476.x.
5. Di Paola A, Marrapodi MM, Di Martino M, Giliberti G, Di Feo G, Rana D, et al. Bone health impairment in patients with hemoglobinopathies: from biological bases to new possible therapeutic strategies. Int J Mol Sci. 2024;25(5):2902. https://doi.org/10.3390/ijms25052902.
6. Dalle Carbonare L, Mattè A, Valenti MT, Siciliano A, Mori A, Schweiger V, et al. Hypoxia-reperfusion affects osteogenic lineage and promotes sickle cell bone disease. Blood. 2015;126(20):2320–8. https://doi.org/10.1182/blood-2015-04-641969.
7. Steinberg MH. Fetal hemoglobin in sickle cell anemia. Blood. 2020;136(21):2392–400. https://doi.org/10.1182/blood.2020007645.
8. Nouraie M, Lee JS, Zhang Y, Kanias T, Zhao X, Xiong Z, et al. The relationship between the severity of hemolysis, clinical manifestations and risk of death in 415 patients with sickle cell anemia in the US and Europe. Haematologica. 2013;98(3):464–72. https://doi.org/10.3324/haematol.2012.068965.
9. Nouraie M, Cheng K, Niu X, Moore-King E, Fadojutimi-Akinsi MF, Minniti CP, et al. Predictors of osteoclast activity in patients with sickle cell disease. Haematologica. 2011;96(8):1092–8. https://doi.org/10.3324/haematol.2011.042499.
10. Souza SFC, de Carvalho HLCC, Costa CPS, Thomaz EBAF. Association of sickle cell haemoglobinopathies with dental and jaw bone abnormalities. Oral Dis. 2018;24(3):393–403. https://doi.org/10.1111/odi.12742.
11. Faber TD, Yoon DC, White SC. Fourier analysis reveals increased trabecular spacing in sickle cell anemia. J Dent Res. 2002;81(3):214–8. https://doi.org/10.1177/0810214.
12. Demirbaş AK, Ergün S, Güneri P, Aktener BO, Boyacıoğlu H. Mandibular bone changes in sickle cell anemia: fractal analysis. Oral Surg Oral Med Oral Pathol Oral Radiol Endod. 2008;106(1):e41–8. https://doi.org/10.1016/j.tripleo.2008.03.007.
13. Basavarajappa S, Konddajji Ramachandra V, Kumar S. Fractal dimension and lacunarity analysis of mandibular bone on digital panoramic radiographs of tobacco users. J Dent Res Dent Clin Dent Prospects. 2021;15(2):140–6. https://doi.org/10.34172/joddd.2021.024.
14. de Sá Cavalcante D, da Silva Castro MG, Quidute ARP, Martins MRA, Cid AMPL, de Barros Silva PG, et al. Evaluation of bone texture imaging parameters on panoramic radiographs of patients with Sheehan's syndrome: a STROBE-compliant case-control study. Osteoporos Int. 2019;30(11):2257–69. https://doi.org/10.1007/s00198-019-05086-4.
15. Santos DBN, Dos Santos BCO, da Silva LC, Dos Santos MPA, Munhoz L, de Andrade BAB, et al. Mandibular radiographic assessment in sickle cell disease: a systematic review of radiomorphometric indices and fractal dimension. Spec Care Dentist. 2026;46(3):e70186. https://doi.org/10.1111/scd.70186.
16. Baxter-Jones ADG, Faulkner RA, Forwood MR, Mirwald RL, Bailey DA. Bone mineral accrual from 8 to 30 years of age: an estimation of peak bone mass. J Bone Min Res. 2011;26(8):1729–39. https://doi.org/10.1002/jbmr.412.
17. Schneider CA, Rasband WS, Eliceiri KW. NIH Image to ImageJ: 25 years of image analysis. Nat Methods. 2012;9(7):671–5. https://doi.org/10.1038/nmeth.2089.
18. Ferreira T, Rasband WS, ImageJ User Guide. IJ 1.46r. Bethesda (MD): National Institutes of Health; 2012. https://imagej.net/ij/docs/guide/. Accessed 16 Oct 2026.
19. White SC, Rudolph DJ. Alterations of the trabecular pattern of the jaws in patients with osteoporosis. Oral Surg Oral Med Oral Pathol Oral Radiol Endod. 1999;88(5):628–35. https://doi.org/10.1016/S1079-2104(99)70097-1.
20. Karperien A. FracLac for ImageJ: user's guide. Charles Sturt University; 2007–2012. https://imagej.net/ij/plugins/fraclac/FLHelp/Introduction.htm. Accessed 16 Oct 2026.
21. Arganda-Carreras I, Fernández-González R, Muñoz-Barrutia A, Ortiz-de-Solorzano C. 3D reconstruction of histological sections: application to mammary gland tissue. Microsc Res Tech. 2010;73(11):1019–29. https://doi.org/10.1002/jemt.20829.
22. Giordano P, Urbano F, Lassandro G, Faienza MF. Mechanisms of bone impairment in sickle bone disease. Int J Environ Res Public Health. 2021;18(4):1832. https://doi.org/10.3390/ijerph18041832.
23. Almeida VSM, Soares MQS, Leite-Ribeiro PM, Rubira-Bullen IRF, Lins-Kusterer LEF, Sarmento VA. Evaluation of mandibular bone microstructure in CT scans of people with sickle cell disease. Eur J Dent. 2024;18(1):356–9. https://doi.org/10.1055/s-0043-1771200.
24. Neves FS, Oliveira LSAF, Torres MGG, Toralles MBP, da Silva MCBO, Campos MIG, et al. Evaluation of panoramic radiomorphometric indices related to low bone density in sickle cell disease. Osteoporos Int. 2012;23(7):2037–42. https://doi.org/10.1007/s00198-011-1810-z.
25. Tosoni GM, Lurie AG, Cowan AE, Burleson JA. Pixel intensity and fractal analyses: detecting osteoporosis in perimenopausal and postmenopausal women by using digital panoramic images. Oral Surg Oral Med Oral Pathol Oral Radiol Endod. 2006;102(2):235–41. https://doi.org/10.1016/j.tripleo.2005.08.020.
26. Oliveira ML, Pedrosa EFNC, Cruz AD, Haiter-Neto F, de Paula FJA, Watanabe PCA. Relationship between bone mineral density and trabecular bone pattern in postmenopausal osteoporotic Brazilian women. Clin Oral Investig. 2013;17(8):1847–53. https://doi.org/10.1007/s00784-012-0882-2.
27. Palma LF, Tateno RY, Remondes CM, Marcucci M, Cortes ARG. Impact of radiotherapy on mandibular bone: a retrospective study of digital panoramic radiographs. Imaging Sci Dent. 2020;50(1):31–6. https://doi.org/10.5624/isd.2020.50.1.31.
28. Palma LF, Serrano RV, Campos L, Marcucci M, de Moraes LO. Radiotherapy-induced alterations in trabecular microarchitecture and bone mass of the mandibular condylar process: a retrospective analysis using fractal dimension and pixel intensity on digital panoramic radiographs. Imaging Sci Dent.

2026;56(2):170–5. https://doi.org/10.5624/isd.20250314.
29. Yıldızer E, Sari SK, Peker F, Erdogan AR, Sancak K, Ertem SY. Assessment of mandibular bone architecture in patients with endocrine disorders using fractal dimension and histogram analysis. Tomography. 2025;11(6):70. https://doi.org/10.3390/tomography11060070.
30. Amouriq Y, Guédon J, Normand N, Arlicot A, Benhdech Y, Weiss P. Bone texture analysis on dental radiographic images: results with several angulated radiographs on the same region of interest. Proc SPIE. 2011;7965:796525. https://doi.org/10.1117/12.878152.
31. Yaşar F, Akgünlü F. Fractal dimension and lacunarity analysis of dental radiographs. Dentomaxillofac Radiol. 2005;34(5):261–7. https://doi.org/10.1259/dmfr/85149245.
32. Temur KT, Magat G, Yılmaz M, Ozcan S. Evaluation of the effect of sickle cell disease on the mandibular bone of children and adolescents by image texture and radiomorphometric analysis. Oral Radiol. 2023;39(4):792–801. https://doi.org/10.1007/s11282-023-00704-8.
33. Serindere G, Belgin CA. Evaluation of the effects of hemoglobinopathies on the mandible with fractal dimension analysis. Niger J Clin Pract. 2019;22(10):1435–40. https://doi.org/10.4103/njcp.njcp_196_19.
34. Seiller J, Merle B, Fort R, Virot E, Poutrel S, Cannas G, et al. Prevalence of bone complications in young patients with sickle cell disease presenting low bone mineral density. Bone. 2024;178:116924. https://doi.org/10.1016/j.bone.2023.116924.
35. Adesina OO, Gurney JG, Kang G, Villavicencio M, Hodges J, Chemaitilly W, et al. Height-corrected low bone density associates with severe outcomes in sickle cell disease: SCCRIP cohort study results. Blood Adv. 2019;3(9):1476–88. https://doi.org/10.1182/bloodadvances.2018026047.
36. Gollamudi J, Karkoska KA, Gbotosho OT, Zou W, Hyacinth HI, Teitelbaum SL. A bone to pick: cellular and molecular mechanisms of bone pain in sickle cell disease. Front Pain Res (Lausanne). 2024;4:1302014. https://doi.org/10.3389/fpain.2023.1302014.
37. Gollamudi J, Wu C, Kang G, Lamonica M, Chen PL, Srinivasan R, et al. Prevalence of low bone mineral density increases with age in sickle cell disease. eJHaem. 2026;7(3):e70306. https://doi.org/10.1002/jha2.70306.
38. Heuchert J, Kozieł SM, Spinek AE. Radiomorphometric indices of the mandible as indicators of decreased bone mineral density and osteoporosis: meta-analysis and systematic review. Osteoporos Int. 2024;35(3):401–12. https://doi.org/10.1007/s00198-023-06949-7.
39. Sarrai M, Duroseau H, D'Augustine J, Moktan S, Bellevue R. Bone mass density in adults with sickle cell disease. Br J Haematol. 2007;136(4):666–72. https://doi.org/10.1111/j.1365-2141.2006.06487.x.
40. Baldanzi G, Traina F, Marques Neto JF, Santos AO, Ramos CD, Saad STO. Low bone mass density is associated with hemolysis in Brazilian patients with sickle cell disease. Clin (Sao Paulo). 2011;66(5):801–5. https://doi.org/10.1590/S1807-59322011000500015.
41. Milton JN, Rooks H, Drasar E, McCabe EL, Baldwin CT, Melista E, et al. Genetic determinants of haemolysis in sickle cell anaemia. Br J Haematol. 2013;161(2):270–8. https://doi.org/10.1111/bjh.12245.
42. Sadat-Ali M, Al-Sultan O, Al-Turki HA, Al Elq AH. Does high serum iron level induce low bone mass in sickle cell anemia? Biometals. 2011;24(1):19–22. https://doi.org/10.1007/s10534-010-9391-4.
43. Coates TD, Wood JC. How we manage iron overload in sickle cell patients. Br J Haematol. 2017;177(5):703–16. https://doi.org/10.1111/bjh.14575.
44. Maheshwari A, Zebaze R, Milat F, Kaplan Z, Wong P. Beyond osteoporosis in sickle cell disease: high bone mineral density, disorganised bone and fracture risk. Intern Med J. 2026. https://doi.org/10.1111/imj.70557.
45. Ogunkunle AK, Mahmud FA, Abubakar MG, Dogara AB, Adanlawo WT, Yusuf R, et al. Diagnostic relevance of osteocalcin and bone alkaline phosphatase as markers of bone turnover in sickle cell anaemia: a Zaria study. Afr Health Sci. 2026;26(2):59–68. https://doi.org/10.4314/ahs.v26i2.8.
46. Adesina OO, Voutsinas J, Wu QV, Teos LY, Rokni M, Nalbant H, et al. Low bone mineral density and pain impact in adults with sickle cell disease. Blood Adv. 2026;10(3):748–58. https://doi.org/10.1182/bloodadvances.2025015957.

Figures

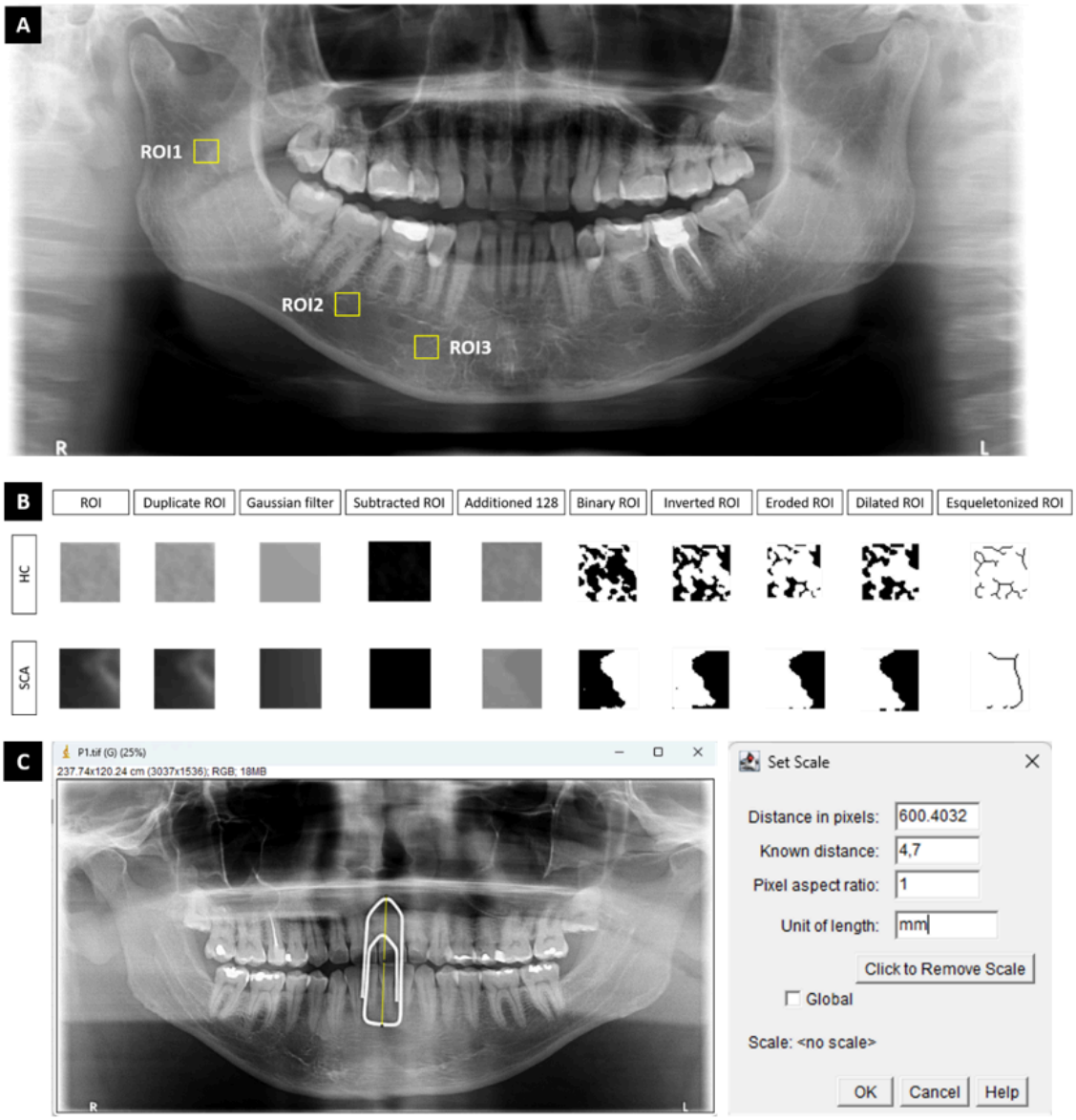


Figure 1

Mandibular regions of interest, image-processing workflow, and spatial calibration.

Figure 1. Selection of mandibular regions of interest and image-processing procedures. (A) Anatomical location of the three mandibular regions of interest (ROI1, ROI2, and ROI3), each standardized to 50 × 50 pixels. (B) Image-processing steps applied to each region of interest for quantitative analysis. (C) Spatial calibration of the panoramic radiograph for conversion of pixels into millimeters.

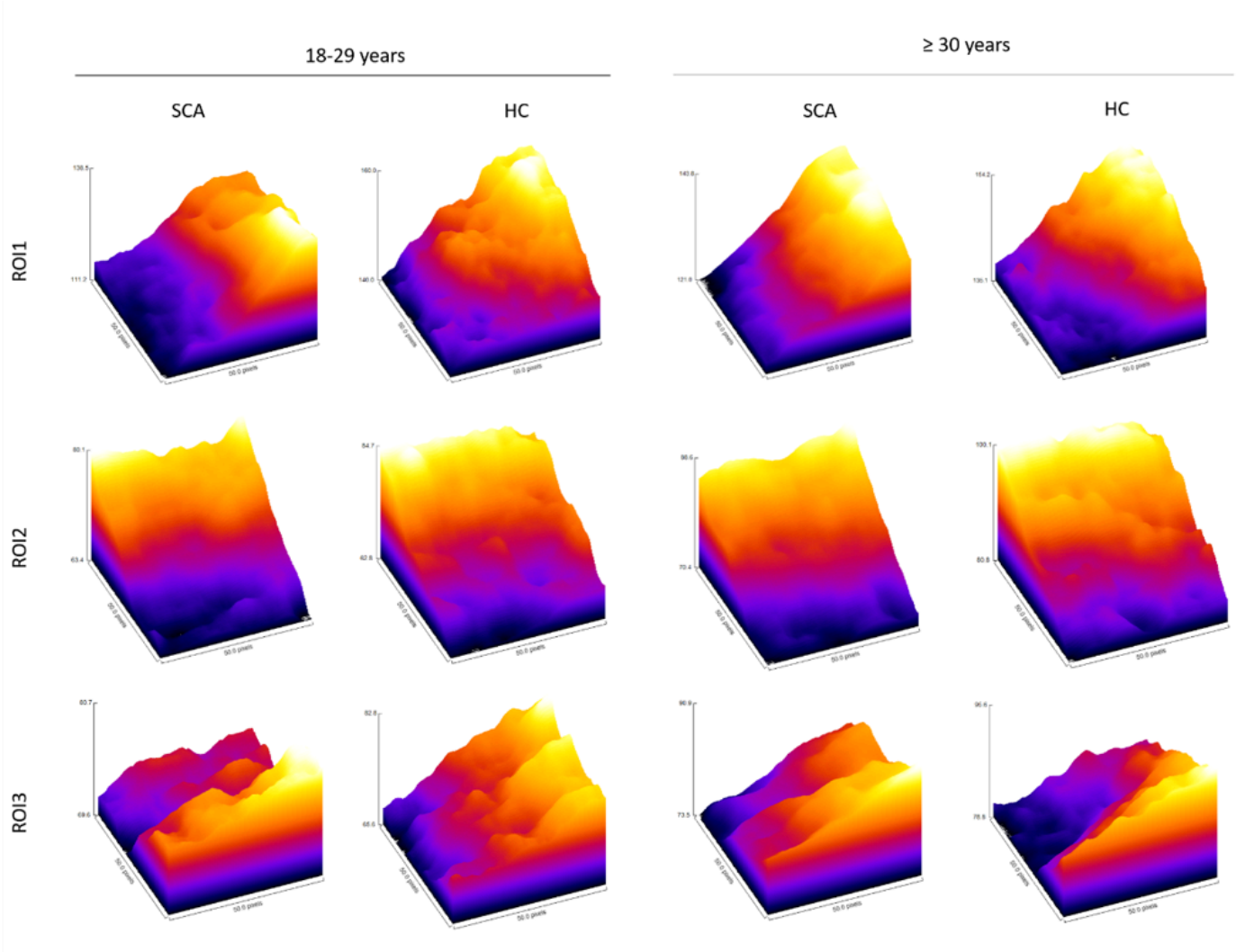


Figure 2

Mean pixel intensity by region, study group, and age category.

Figure 2. Surface plots of mean pixel intensity across regions of interest according to study group and age category. Rows represent ROI1, ROI2, and ROI3; columns show the sickle cell anemia and control groups within the 18–29 and ≥30-year age categories. The horizontal axes represent the spatial dimensions of each region of interest, and the vertical axis represents pixel intensity. Color gradients indicate variations in intensity within each surface. These plots provide a qualitative visualization complementary to the quantitative analysis.

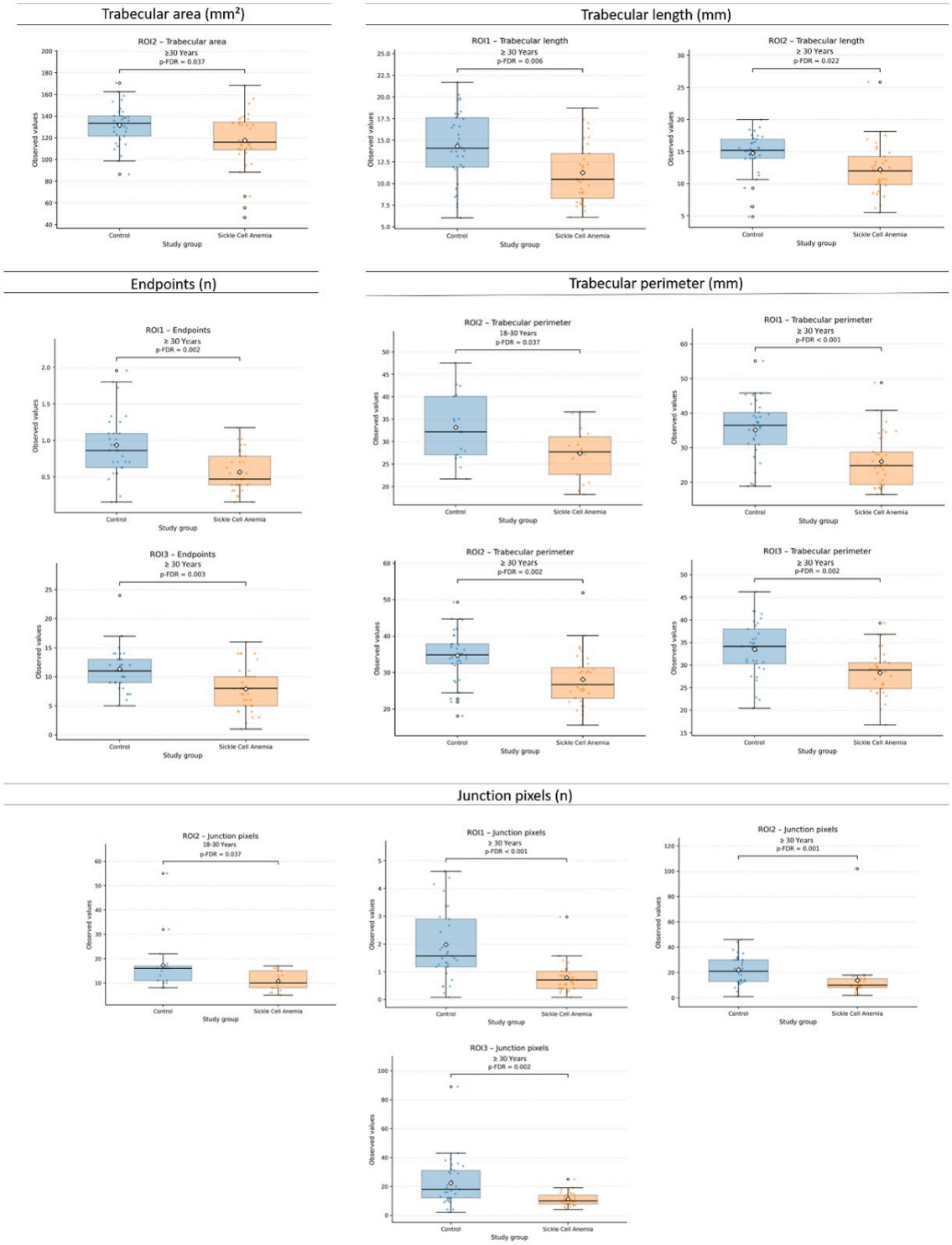


Figure 3

FDR-significant between-group differences in trabecular microarchitecture parameters.

Figure 3. Boxplots of morphometric and trabecular connectivity parameters with significant differences between the Sickle Cell Anemia and control groups after Benjamini–Hochberg correction. Only comparisons with p-FDR < 0.05 are shown. Boxes indicate interquartile ranges, horizontal lines medians, diamonds means, and dots individual participants; brackets display between-group comparisons and corresponding p-FDR values.

Supplementary Files

This is a list of supplementary files associated with this preprint. Click to download.

- SupplementaryFile1.docx
- SupplementaryFile2.docx
- SupplementaryFile3.docx
- SupplementaryFile4.docx